J Physiol 589.18 (2011) pp 4437–4455

The Journal of Physiology

Mechanism of auxiliary β-subunit-mediated membrane targeting of L-type ($Ca_V1.2$) channels

Kun Fang and Henry M. Colecraft

Department of Physiology and Cellular Biophysics, Columbia University, College of Physicians and Surgeons, New York, NY 10032, USA

Non-technical summary Voltage-dependent L-type calcium ($Ca_V1.2$) channels are critical gateways for Ca^{2+} entry into excitable cells such as heart myocytes and neurons. This Ca^{2+} signal controls many essential physiological responses including triggering the heartbeat and regulating gene expression in nerve cells. $Ca_V1.2$ channels are multi-subunit proteins, comprising α_{1C}, β, and $\alpha_2\delta$ subunits, and must target to the cell surface to function. Association of a pore-forming α_{1C} and cytosolic β is necessary for targeting $Ca_V1.2$ channels to the cell surface through poorly understood mechanisms. Here, using a chimeric channel strategy, we provide data that suggest β binding to the α_{1C} intracellular I–II loop causes a global rearrangement of intracellular domains, shifting a balance of power between export signals on the I–II loop and retention signals elsewhere on the channel. The results provide novel insights into the mechanism of a protein–protein interaction that is vital for forming functional $Ca_V1.2$ channels.

Abstract Ca^{2+} influx via Ca_V1/Ca_V2 channels drives processes ranging from neurotransmission to muscle contraction. Association of a pore-forming α_1 and cytosolic β is necessary for trafficking Ca_V1/Ca_V2 channels to the cell surface through poorly understood mechanisms. A prevalent idea suggests β binds the α_1 intracellular I–II loop, masking an endoplasmic reticulum (ER) retention signal as the dominant mechanism for Ca_V1/Ca_V2 channel membrane trafficking. There are hints that other α_1 subunit cytoplasmic domains may play a significant role, but the nature of their potential contribution is unclear. We assessed the roles of all intracellular domains of $Ca_V1.2$-α_{1C} by generating chimeras featuring substitutions of all possible permutations of intracellular loops/termini of α_{1C} into the β-independent $Ca_V3.1$-α_{1G} channel. Surprisingly, functional analyses demonstrated α_{1C} I–II loop strongly increases channel surface density while other cytoplasmic domains had a competing opposing effect. Alanine-scanning mutagenesis identified an acidic-residue putative ER export motif responsible for the I–II loop-mediated increase in channel surface density. β-dependent increase in current arose as an emergent property requiring four α_{1C} intracellular domains, with the I–II loop and C-terminus being essential. The results suggest β binding to the α_{1C} I–II loop causes a C-terminus-dependent rearrangement of intracellular domains, shifting a balance of power between export signals on the I–II loop and retention signals elsewhere.

(Resubmitted 16 June 2011; accepted after revision 5 July 2011; first published online 11 July 2011)

Corresponding author H. M. Colecraft: Columbia University, College of Physicians and Surgeons, Department of Physiology and Cellular Biophysics, 1150 St Nicholas Avenue, 504 Russ Berrie Pavilion, New York, NY 10032, USA. Email: hc2405@columbia.edu

Abbreviations AID, α interaction domain; BBS, bungarotoxin binding site; Ca_V channel, voltage-dependent calcium channel; $Ca_V\beta$, voltage-dependent calcium channel auxiliary β subunit; CaM, calmodulin; CCD, charge-coupled device; CFP, cyan fluorescent protein; C-terminus, carboxyl terminus; ER, endoplasmic reticulum; GK, guanylate kinase; I_{Ca}, calcium channel current; PEER, putative endoplasmic reticulum export region; QD, quantum dot; Q_{max}, maximal gating charge; YFP, yellow fluorescent protein.

DOI: 10.1113/jphysiol.2011.214247

Introduction

The entry of calcium ions into excitable cells through voltage-dependent Ca_V1 ($Ca_V1.1-1.4$) and –2 ($Ca_V2.1-2.3$) channels constitutes a prevalent and versatile signal transduction paradigm in biology. This basic mechanism is used to evoke neurotransmitter release that underlies synaptic transmission (Catterall & Few, 2008), control neuronal excitability by coupling to Ca^{2+}-sensitive K^+ channels (Fakler & Adelman, 2008), trigger excitation–contraction coupling in heart muscle (Bers, 2002), and regulate gene expression (Deisseroth *et al.* 2003). Hence, myriad biological processes critically depend on the proper cell surface targeting and function of Ca_V1/Ca_V2 channels. Functional Ca_V1/Ca_V2 channels are multi-subunit protein complexes containing a membrane-spanning α_1 subunit assembled with auxiliary proteins that include β ($\beta_1-\beta_4$) and $\alpha_2\delta$ ($\alpha_2\delta1-3$) subunits, and calmodulin (Catterall & Few, 2008). While the α_1 subunit contains the voltage sensor and channel pore, its subcellular localization and biophysical properties are profoundly influenced by the accessory proteins. In particular, β subunits are essential determinants of channel behaviour, affecting both trafficking and gating (Dolphin, 2003; Buraei & Yang, 2010). Auxiliary βs induce a hyperpolarizing shift in the voltage dependence of channel activation, increase channel open probability (P_o), and determine channel inactivation properties (Perez-Reyes *et al.* 1992; Neely *et al.* 1993; De Waard & Campbell, 1995; Colecraft *et al.* 2002; Dolphin, 2003; Takahashi *et al.* 2004; Buraei & Yang, 2010). In addition to the biophysical modifications, a cardinal feature of Ca_V1/Ca_V2 channels is their reliance on association with a β for effectual targeting to the cell surface (Gao *et al.* 1999; Dolphin, 2003; Kanevsky & Dascal, 2006; Buraei & Yang, 2010; Obermair *et al.* 2010; Yang *et al.* 2010). Because this trafficking step is fundamental to the formation of functional Ca_V1/Ca_V2 channels, much effort has focused on elucidating how β subunits promote membrane-targeting of Ca_V channels.

$Ca_V\beta$s contain a *src* homology 3 (SH3)/guanylate kinase (GK) structural module (Chen *et al.* 2004; Opatowsky *et al.* 2004; Van Petegem *et al.* 2004), identifying them as members of the membrane-associated guanylate kinase (MAGUK) family of scaffold proteins (Funke *et al.* 2005). The β GK domain binds with high affinity to a conserved 18-residue region (termed the α_1 interaction domain, or AID) in the α_1 subunit intracellular I–II loop (Pragnell *et al.* 1994; Chen *et al.* 2004; Opatowsky *et al.* 2004; Van Petegem *et al.* 2004). Mutations that selectively disrupt the β-AID interaction prevent β-induced channel targeting to the membrane, suggesting a dominant role for this association in regulating Ca_V channel trafficking (Van Petegem *et al.* 2008; Bourdin *et al.* 2010; Buraei & Yang, 2010; Obermair *et al.* 2010). One prevalent idea, based on experiments carried out on $Ca_V2.1$ channels, is that Ca_V1/Ca_V2 α_1 subunits possess an ER retention signal on the I–II loop that is masked upon β-binding, thus allowing forward trafficking of the channel to proceed (Bichet *et al.* 2000). However, several observations challenge the sufficiency and generality of this model to account for β-induced membrane targeting of Ca_V1/Ca_V2 channels (Buraei & Yang, 2010). First, the putative ER retention sequence on the α_1 I–II loop has not been identified in any Ca_V1/Ca_V2 channel (Bichet *et al.* 2000). Second, in contrast to $Ca_V2.1$, neither the $Ca_V1.2$ nor $Ca_V2.2$ α_1 subunit I–II loop displayed ER retention properties when fused to CD4 (Altier *et al.* 2011). Third, deletions in the $Ca_V1.2$ α_{1C} C-terminus that do not impact β binding to the channel can, nevertheless, severely diminish membrane trafficking (Gao *et al.* 2000). Fourth, point mutations in the α_{1C} C-terminus that disrupt apo-calmodulin, but not β subunit binding, also significantly impair channel trafficking (Wang *et al.* 2007; Bourdin *et al.* 2010). These discrepancies underscore a clear need for a unifying model that accounts for both the essential role of β binding to the I–II loop and the apparent importance of the C-terminus for $Ca_V1.2$ channel membrane trafficking. Furthermore, the potential contribution of other α_1 subunit intracellular domains (N-terminus, II–III loop, and III–IV loop) to β-induced trafficking has not been rigorously explored in any Ca_V1/Ca_V2 channel. This omission critically compromises the necessary dataset required to formulate a more complete model of β-induced trafficking of Ca_V1/Ca_V2 channels.

Identifying whether and how the various intracellular domains of α_1 contribute to β-dependent channel trafficking is a daunting task given their multiplicity and likely complex three-dimensional spatial arrangement. One typical approach to the problem has been to mutate or delete portions of α_1 intracellular domains and assess whether they compromise channel trafficking (Bichet *et al.* 2000; Wang *et al.* 2007). While such loss-of-function approaches provide important information about channel regions that may be involved in trafficking, the dataset produced typically yield only modest insights into the mechanistic basis for β-dependent regulation of Ca_V channel trafficking. For example, observations that deletions in the $Ca_V1.2$ α_{1C} C-terminus may impair channel trafficking simply informs that this intracellular domain is important for the process, but not how it is involved. An alternative reductionist approach involves splicing individual α_1 subunit intracellular domains to the C-terminus of the trans-membrane protein CD8 (or CD4) and observing how they impact targeting of this protein to the cell surface (Bichet *et al.* 2000; Cornet *et al.* 2002; Wang *et al.* 2007; Altier *et al.* 2011). This is a useful method that, nevertheless, suffers from two main disadvantages. First, in the context of the channel, three of the α_1 intracellular

loops (the I–II, II–III, and III–IV loops) are geometrically constrained by having transmembrane regions bracketing either side. This configuration is lost when the loops are fused to CD8, and the resulting change in conformation could impact their functional properties. Second, this approach neglects possible interactions among the α_1 intracellular domains that could give rise to new emergent properties.

Here, we took a gain-of-function chimeric channel approach seeking to reconstitute β-dependent trafficking in a normally β-independent channel. While the chimeric channel strategy has its own inherent limitations, the approach offered the potentially unique advantage that Ca_V channel α_1 subunit intracellular domains could be used in a manner that preserved their conformations and spatial inter-relationships. This was achieved by systematically generating a series of 31 separate chimeric channels featuring a swap of all possible permutations of the intracellular domains of the β-dependent $Ca_V1.2$ α_{1C} into the analogous positions in the β-independent $Ca_V3.1$ channel α_{1G} subunit. Functional analyses of these chimeras yielded results that provided a different perspective of the determinants underlying β-mediated membrane trafficking of $Ca_V1.2$ channels, and suggest a new mechanistic model for this physiologically crucial phenomenon.

Methods

Generation of plasmid constructs

All the experiments comply with the policies and regulations of *The Journal of Physiology* given by Drummond (2009). Generation of plasmids encoding α_{1C}[BBS]–yellow fluorescent protein (YFP) and β_{2a}–cyan fluorescent protein (CFP) have been previously described (Yang *et al.* 2010). Chimeric channels featuring a systematic swap of intracellular domains of rabbit $Ca_V1.2$ α_{1C} (accession no.: X15539) into the rat $Ca_V3.1$ α_{1G} (accession no.: AF027984) backbone were generated using the in-fusion cloning technique (Clontech, Mountain View, CA, USA) according to the manufacturer's instructions. To generate chimeras in which only one intracellular domain of α_{1G}-YFP was replaced by the corresponding intracellular domain from α_{1C}, four specially designed primers were used – two primers for PCR amplification of the vector containing the α_{1G} segment, and two primers for PCR amplification of the relevant α_{1C} segment as the insert (online Supplemental Material, Table S1). The in-fusion reaction was carried out with purified vector and insert in a 1:2 molar ratio, and the resulting chimeric constructs subsequently cloned. Replacement of multiple intracellular domains was achieved by combining the in-fusion technique with traditional restriction enzyme digestion and ligation methods. The precise boundaries of the N- and C-termini, and the intracellular loops of $Ca_V1.2$ and $Ca_V3.1$ used to generate the chimeras are shown in the online Supplemental Material, Fig. S1.

To generate C-terminus-truncated α_{1C}[BBS]-YFP constructs, we used PCR to introduce a *Xho*I site immediately downstream of the sequence for the last desired residue (G1540, D1632, L1732, or K1906) in the context of α_{1C}[BBS]. YFP was then PCR amplified and cloned in-frame and downstream of truncated α_{1C} using *Xho*I and *Xba*I sites. Point mutations changing acidic residues (D or E) to alanines in the α_{1C} I–II loop were accomplished using the QuikChange Lightning Site-Directed Mutagenesis Kit (Stratagene) according to manufacturer's instructions. All constructs were verified by sequencing.

Cell culture and transfection

Low-passage-number human embryonic kidney (HEK) 293 cells were maintained in Dulbecco's modified Eagle's medium (DMEM) supplemented with 10% fetal bovine serum (FBS) and 100 μg ml^{-1} penicillin–streptomycin at 37°C. HEK 293 cells were transiently transfected with appropriate constructs – 6 μg wild-type or modified α_{1C} or α_{1G}, 6 μg β_{2a} (as needed), and 1 μg T antigen using calcium phosphate precipitation – and cultured in supplemented DMEM at 37°C for 48–72 h before use.

Electrophysiology

Whole-cell recordings were conducted 48–72 h after transfection using an EPC-10 patch clamp amplifier (HEKA Electronics, Lambrecht, Germany) controlled by PULSE software (HEKA). Micropipettes were prepared from 1.5 mm thin-walled glass (World Precision Instruments, Sarasota, FL, USA) with a filament micropipette puller (P-97, Sutter Instrument Co., Novato, CA, USA). The internal solution contained (in mM): 135 caesium methanesulphonate ($MeSO_3$), 5 CsCl, 5 EGTA, 1 $MgCl_2$, 4 MgATP (added fresh) and 10 Hepes (pH 7.3). External solution contained (in mM): 140 tetraethylammonium-$MeSO_3$, 5 $BaCl_2$ and 10 Hepes (pH 7.4). When filled with internal solution, the resistance of the pipette was typically 1.5–2 MΩ. Whole-cell I–V curves were generated from a family of step depolarizations (−50 to +50 mV from a holding potential of −90 mV for α_{1C} constructs, or −100 to +40 mV from a holding potential of −100 mV for wild-type α_{1G} and chimeric constructs). Currents were sampled at 25 kHz and filtered at 5 or 10 kHz. Traces were acquired at a repetition interval of 6 s. Leak and capacitive currents were subtracted using a P/8 protocol. I–V curves from individual cells were fit using a least-squares method to the following modified

Boltzmann equation:

$$I = G(V - V_{rev})\frac{1}{1 + \exp\left(\frac{V_{0.5} - V}{k}\right)}$$

where, G is the specific conductance, V_{rev} is the reversal potential, $V_{0.5}$ is the potential of half-maximal activation, and k is a slope factor.

Detection and quantification of cell surface Cav1.2 channels with quantum dots

Relative surface expression of epitope-tagged α_{1C} subunits was quantitatively determined using quantum dot labelling and flow cytometry as previously described (Yang *et al.* 2010). Briefly, HEK 293 cells transfected with BBS-tagged α_{1C}-YFP constructs in six-well tissue culture dishes were washed twice with phosphate-buffered saline (PBS) containing Ca^{2+} and Mg^{2+}, and sequentially incubated with 1 μM biotinylated α-bungarotoxin (BTX) in DMEM–3% BSA at room temperature for 1 h and 5 nM streptavidin-conjugated quantum dot (QD_{655}, Invitrogen) at 4°C for 1 h in the dark. Surface labelled HEK 293 cells were harvested with trypsin, washed with PBS and assayed by flow cytometry using a BD LSRII Cell Analyzer (BD Biosciences, San Jose, CA, USA). CFP- and YFP-tagged proteins were excited at 407 and 488 nm, respectively, and red quantum dot signal was excited at 633 nm. For each group of experiments, we used isochronal untransfected and single colour controls to manually set the appropriate gain settings for each fluorophore to ensure signals remained in the linear range, and to set threshold values. The same gain settings were then used for assaying all isochronal transfection samples.

Flow cytometry data were analysed using FlowJo software. To normalize for protein expression, analysis of QD fluorescence was conducted over a window selected such that the mean YFP fluorescence intensity registered 1000 arbitrary units across all groups. In the case of $\alpha_{1C}\Delta$1632-YFP and $\alpha_{1C}\Delta$1540-YFP, there was an apparent decrease in protein expression. Therefore, for these constructs the comparisons to control were done over an analysis window with a mean YFP fluorescence intensity of 400 arbitrary units (Supplemental Material, Fig. S6). For each experimental condition, the ratio of the mean QD fluorescence intensity to the mean YFP fluorescence intensity ($R_{QD/YFP}$) was calculated and normalized to the $R_{QD/YFP}$ obtained for isochronal control cells expressing $\alpha_{1C}+\beta_{2a}$ channels.

Fluorescence imaging

Fluorescence images of labelled (YFP and quantum dot) HEK 293 cell suspensions were obtained using an inverted Nikon Eclipse Ti microscope equipped for epifluorescence. Fluorophores were excited with the appropriate wavelength using a DeltaRAM Random Access Monochromator (Photon Technology International, Birmingham, NJ, USA) and the emitted light imaged with a QuantEM CCD camera (Roper Scientific, Trenton, NJ, USA).

Western blotting

Transiently transfected HEK 293 cells were harvested with trypsin, washed with PBS and solubilized in lysis buffer (20 mM Tris base, 1 mM EDTA, 150 mM NaCl, 1% SDS, 0.1% Triton X-100, pH 7.5), supplemented with Complete Mini protease inhibitor cocktail (Roche), by brief sonication. Protein concentrations of the cell lysates were determined with Pierce BCA Protein Assay Kit (Thermo Scientific). Following addition of sample buffer (50 mM Tris base, 10% glycerol, 2% sodium dodecyl sulfate (SDS), 50 mM dithiothreitol (DTT), 0.2 mg ml^{-1} bromphenol blue, pH 7.5), cell lysates were resolved by SDS–PAGE (NuPage 10% gel, Invitrogen) at a constant voltage of 200 V for 1 h. Protein bands were then electrotransferred to a 0.45 μm nitrocellulose membrane for 2.5 h at 4°C at a constant voltage of 30 V in transfer buffer (96 mM glycine, 12 mM Tris base, 0.01% SDS, 20% methanol, pH 8.3). The membranes were blocked for 1 h at room temperature with 5% milk in TBS-T buffer (20 mM Tris base, 140 mM NaCl, 0.1% Tween-20, pH 7.6) and incubated overnight at 4°C with rabbit anti-GFP antibody (1:10,000) in TBS-T. The blots were washed with TBS-T and incubated with goat anti-rabbit antibody (1:10,000) for 1 h at room temperature. After further washing, the immune complexes were visualized using SuperSignal West Pico Chemiluminescent Substrate (Thermo Scientific).

Data and statistical analyses

Electrophysiological data were analysed off-line using built in functions in PulseFit (HEKA), Microsoft Excel and Origin software. Statistically significant differences between means ($P < 0.05$) were determined using one-way ANOVA followed by pairwise comparisons using the Bonferroni test for multiple group comparisons, and either Student's unpaired t test or Wilcoxon's rank sum test for comparisons between two groups. Data are presented as means ± SEM.

Results

Differential impact of $Ca_V\beta$ on functional expression of $Ca_V1.2$ (α_{1C}) and $Ca_V3.1$ (α_{1G}) channels

We examined the impact of auxiliary β subunits on functional expression of $Ca_V1.2$ and $Ca_V3.1$ channels reconstituted in HEK 293 cells by transient transfection. Cells transfected with the $Ca_V1.2$ α_{1C}-YFP subunit alone displayed barely detectable currents across the

relevant range of test pulse potentials (Fig. 1*A* and *B*). Co-expression of α_{1C}-YFP with β_{2a}-CFP resulted in a dramatic 15-fold increase in whole-cell current amplitude, accompanied by a 10 mV hyperpolarizing shift in the voltage dependence of channel activation (Fig. 1*A* and *B*; Table 1). $Ca_V1.2$ channels activated at a threshold voltage of −30 mV and peaked at either 0 mV (with β_{2a}) or +10 mV (no β) (Fig. 1*A* and *B*). In sharp contrast, cells transfected with $Ca_V3.1$ α_{1G}-YFP subunit alone displayed large whole-cell currents that activated at a threshold potential of −60 mV and peaked at −30 mV (Fig. 1*C* and *D*), consistent with its classification as a low voltage-activated calcium channel (Perez-Reyes *et al.* 1998). Co-expression of α_{1G}-YFP with β_{2a}-CFP had no impact on either the whole-cell current amplitude or the voltage dependence of channel gating compared to cells expressing α_{1G} alone (Fig. 1*C* and *D*; Table 1). These results recapitulate the well-known impact of β subunits on the functional expression of high-voltage-activated Ca_V1 and Ca_V2 channels, and the relative β independence of low voltage-activated Ca_V3 channels.

In mammalian cells, β subunits markedly enhance the membrane trafficking of Ca_V1/Ca_V2 channels to the plasma membrane, and this represents a major

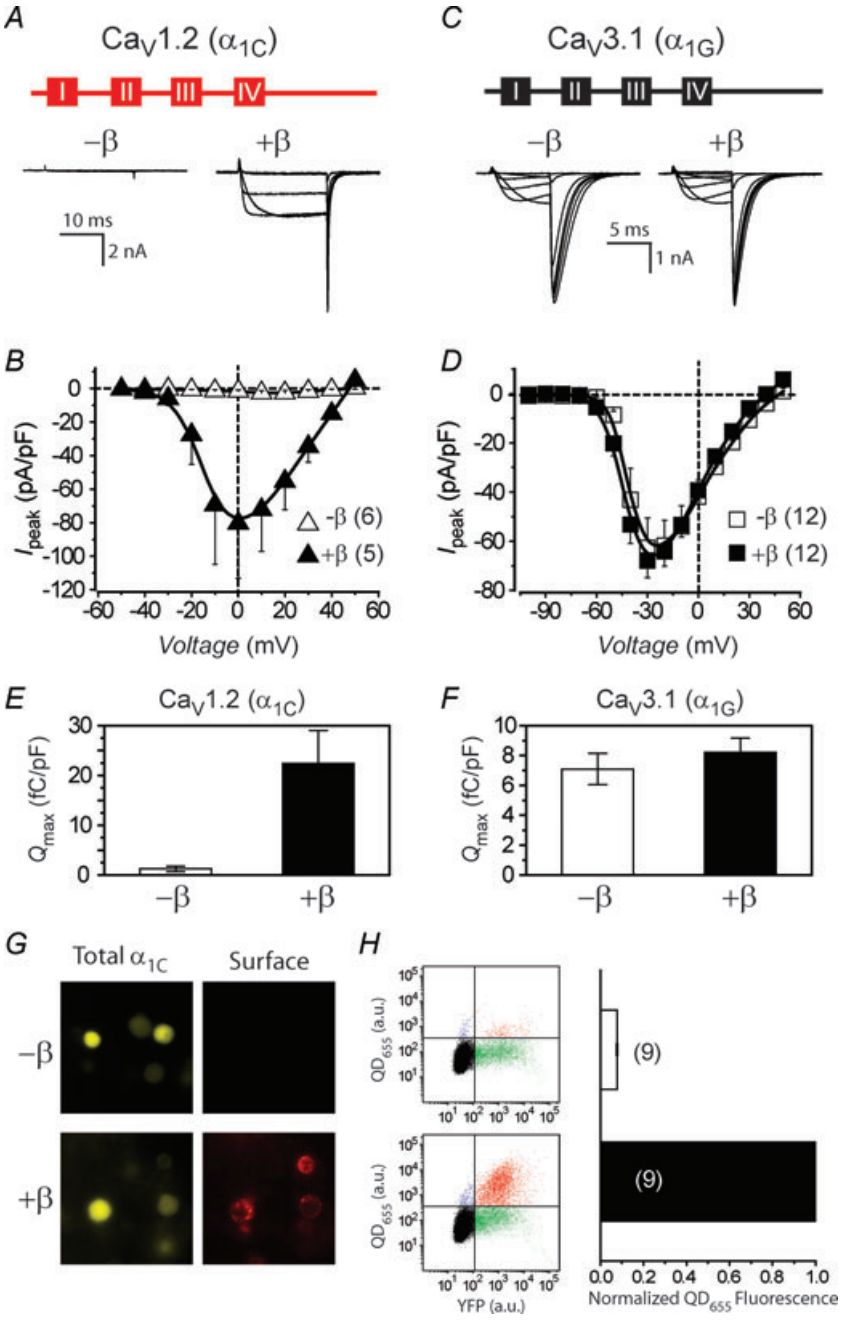

Figure 1. Divergent regulation of $Ca_V1.2$ and $Ca_V3.1$ channels by auxiliary β subunits
A, top, schematic diagram illustrating topology of $Ca_V1.2$ α_{1C} subunit. Four homologous transmembrane domains (boxes labelled I–IV) are connected and flanked by five intracellular modules (red lines). Bottom, exemplar whole-cell currents from $Ca_V1.2$ channels reconstituted without (left) or with (right) auxiliary β subunits. Displayed currents were elicited by voltage steps to −30, −10, +10 and +30 mV. *B*, population peak current density versus voltage (*I*–*V*) relationship for $Ca_V1.2$ channels reconstituted with either α_{1C} alone (△, $n = 6$ for each point) or $\alpha_{1C} + \beta_{2a}$ (▲, $n = 5$). *C*, top, topological illustration of $Ca_V3.1$ α_{1G} subunit. Bottom, exemplar currents from $Ca_V3.1$ channels reconstituted without (left) or with (right) auxiliary β subunits. *D*, population *I*–*V* relationship for $Ca_V3.1$ channels reconstituted with either α_{1G} alone (□, $n = 12$) or $\alpha_{1G} + \beta_{2a}$ (■, $n = 12$). *E*, fluorescence images of HEK 293 cells expressing either α_{1C}[BBS]-YFP alone (top) or α_{1C}[BBS]-YFP + β_{2a} (bottom). Left, YFP fluorescence shows total α_{1C} expressed in the cells. Right, quantum dot (QD_{655}) fluorescence specifically labels α_{1C} channels at the cell surface. *F*, left, representative flow cytometry results from live HEK 293 cells transiently transfected with either α_{1C}[BBS]-YFP alone (top) or α_{1C}[BBS]-YFP + β_{2a} (bottom), and with surface channels labelled with QD_{655}. Right, relative surface density of $Ca_V1.2$ channels as reported by normalized QD_{655} fluorescence intensity.

Table 1. Gating parameters for reconstituted channels

Construct	G_{max} (pS)	$V_{0.5}$ (mV)	k	n
α_{1C}	0.19 ± 0.12	13.91 ± 11.36	13.59 ± 3.78	6
$\alpha_{1C} + \beta_{2a}$	1.98 ± 0.70†	−7.81 ± 2.95	6.19 ± 0.83	5
α_{1G}	0.96 ± 0.15	−38.86 ± 0.90	5.10 ± 0.49	12
$\alpha_{1G} + \beta_{2a}$	1.04 ± 0.09	−43.45 ± 1.59	4.56 ± 0.23	12
α_{1G}[cgggg]	0.23 ± 0.10*	−35.09 ± 4.47	13.57 ± 7.20	6
α_{1G}[cgggg] + β_{2a}	0.19 ± 0.07	−41.92 ± 3.30	6.68 ± 1.37	4
α_{1G}[gcggg]	4.08 ± 0.70*	−68.61 ± 1.75*	1.25 ± 0.35*	8
α_{1G}[gcggg] + β_{2a}	1.35 ± 0.23†	−69.76 ± 2.37	1.24 ± 0.53	5
α_{1G}[ggcgg]	0.55 ± 0.12	−40.39 ± 0.52	5.59 ± 0.20	10
α_{1G}[ggcgg] + β_{2a}	0.35 ± 0.09	−39.07 ± 1.16	5.67 ± 0.24	10
α_{1G}[gggcg]	0.17 ± 0.06*	−33.26 ± 1.55*	7.71 ± 0.94*	7
α_{1G}[gggcg] + β_{2a}	0.23 ± 0.11	−33.82 ± 1.55	6.57 ± 1.05	6
α_{1G}[ggggc]	0.30 ± 0.12*	−38.65 ± 2.08	7.89 ± 1.33*	8
α_{1G}[ggggc] + β_{2a}	0.21 ± 0.11	−44.43 ± 2.64	7.40 ± 0.33	4

†$P < 0.05$ compared to the corresponding $-\beta$ data, Wilcoxon's rank sum test. *$P < 0.05$ compared to α_{1G} data using Wilcoxon's rank sum test.

mechanistic contributor to the β-induced increase in whole-cell current amplitude. This effect of β on $Ca_V1.2$ channels can be readily demonstrated in our reconstituted system in two independent ways. First, the maximal gating current recorded in cells expressing α_{1C} either in the absence or the presence of β provides a measure of the number of channels with moveable voltage sensors in the membrane (Neely *et al.* 1993; Takahashi *et al.* 2004). Hence, based on the assumption that β subunits do not alter the unitary gating charge required to open the channel, the time integral of the maximum gating charge (Q_{max}) provides an index of the number of channels in the membrane. Using this metric, cells expressing α_{1C}-YFP + β_{2a}-CFP display a significantly larger Q_{max}, and, therefore, more surface channels than cells transfected with α_{1C}-YFP alone (Fig. 1*E*). By contrast, β_{2a}-CFP had no effect on Q_{max} obtained from cells expressing α_{1G} subunits (Fig. 1*F*), fitting with the lack of impact of the auxiliary subunit on whole-cell current amplitude in $Ca_V3.1$ channels. A second, more direct way of visualizing $Ca_V1.2$ channels at the membrane involves labelling cell surface channels with quantum dots followed by quantification of signals using flow cytometry (Yang *et al.* 2010). Here, a 13-residue bungarotoxin-binding site (BBS) (Sekine-Aizawa & Huganir, 2004) is introduced into the extracellular domain II S5–S6 loop of α_{1C}-YFP, and surface channels are selectively labelled in non-permeabilized cells by sequential exposure to biotinylated bungarotoxin and streptavidin-conjugated quantum dot (Fig. 1*G*). The relative cell surface density of $Ca_V1.2$ channels is then quantified in a high throughput manner by flow cytometry. Using this method, the presence of β_{2a}-CFP resulted in a 12-fold increase in QD_{655} fluorescence intensity compared to cells expressing BBS epitope-tagged α_{1C}-YFP alone (Fig. 1*H*).

The stark contrast between $Ca_V1.2$ α_{1C} and $Ca_V3.1$ α_{1G} subunits could potentially be exploited to identify the important determinants and mechanisms underlying β-dependent trafficking. Given that the β subunit is entirely intracellular, we hypothesized that cytoplasmic domains of the α_{1C} subunit play a prominent role in $Ca_V1.2$ channel ER retention and β-dependent ER export. Accordingly, we systematically generated 31 separate chimeric channels featuring all possible permutations of the five α_{1C} intracellular domains (N-terminus, I–II loop, II–III loop, III–IV loop and C-terminus) swapped into the analogous regions of α_{1G} and assessed the resulting functional outcomes.

Functional outcomes of single intracellular domain-substituted chimeras

We first investigated whether a single α_{1C} subunit intracellular domain could potentially confer ER retention and β-dependent ER export when transplanted into α_{1G}. We generated five individual chimeras (termed α_{1G}[cgggg], α_{1G}[gcggg], α_{1G}[ggcgg], α_{1G}[gggcg] and α_{1G}[ggggc]) in which just one intracellular region of α_{1C} was swapped into the α_{1G} backbone (Fig. 2). We adopted a naming convention in which the backbone channel subunit is followed by a square bracket containing letters that denote the configuration of the intracellular domains. Hence, for example, α_{1G}[cgggg] refers to the chimeric channel in which the N-terminus of α_{1G} is replaced with the analogous segment from α_{1C}. To assess the functional impact of the single-domain substitutions, we transiently expressed the chimeric channels in HEK 293 cells in either the absence or the presence of β_{2a}-CFP and recorded whole-cell currents (Fig. 2). All chimeras, here and throughout, were tagged with YFP enabling

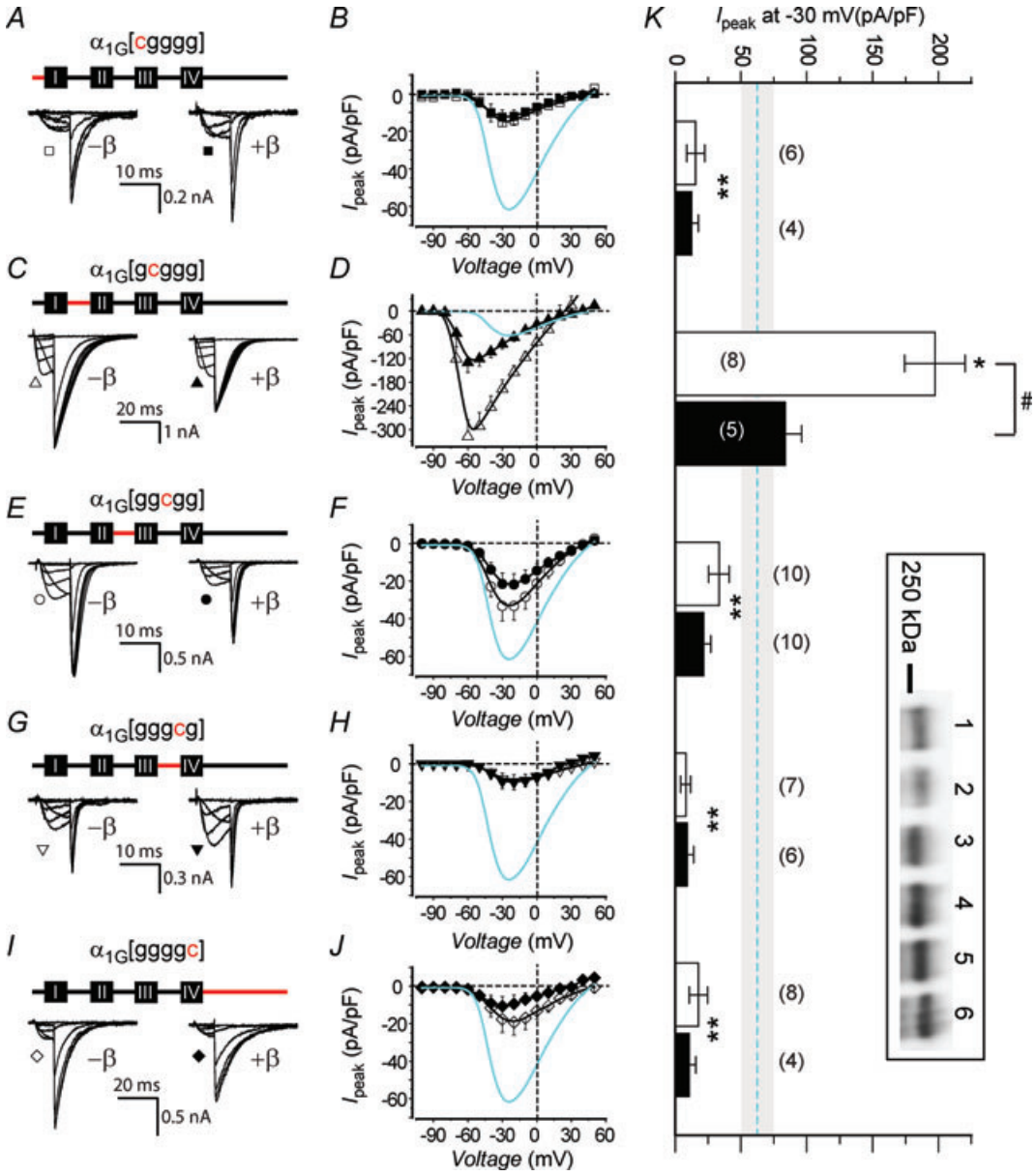

Figure 2. Functional outcomes of chimeras featuring substitutions of individual intracellular domains from $Ca_V1.2$ α_{1C} into $Ca_V3.1$ α_{1G} subunit

A, top, topological illustration of the chimeric channel α_{1G}[cgggg], which features the sole substitution of the α_{1C} N-terminus into α_{1G}. Bottom, exemplar whole-cell currents from cells expressing either α_{1G}[cgggg] alone (left) or α_{1G}[cgggg] + β_{2a} (right). Displayed currents were elicited by voltage steps to −50, −30, −10 and +10 mV. *B*, *I*–*V* curves for channels reconstituted with α_{1G}[cgggg] alone (□) or α_{1G}[cgggg] + β_{2a} (■). Data for wild-type α_{1G} (cyan trace) have been reproduced to facilitate direct visual comparison. *C*–*J*, topological illustrations, exemplar currents and population *I*–*V* relationships for the remaining single intracellular domain substituted chimeras α_{1G}[gcggg], α_{1G}[ggcgg], α_{1G}[gggcg] and α_{1G}[ggggc], respectively. Same format as *A* and *B*. *K*, comparison of peak current densities acquired at −30 mV for the various chimeras in the absence and presence of β_{2a}. The average current density at −30 mV for wild-type α_{1G} alone channels is represented (cyan dashed line) to facilitate visual comparison. $^{**}P < 0.005$ for grouped data ($\pm\beta_{2a}$) compared to α_{1G} ($\pm\beta_{2a}$) using one-way ANOVA followed by means comparisons using the Bonferroni test. $^{*}P < 0.001$ compared to α_{1G} ($\pm\beta_{2a}$), one-way ANOVA followed by Bonferroni test. #$P < 0.05$, Wilcoxon's rank sum test. Inset, Western blot: 1-α_{1G}; 2-α_{1G}[cgggg]; 3-α_{1G}[gcggg]; 4-α_{1G}[ggcgg]; 5-α_{1G}[gggcg]; 6-α_{1G}[ggggc].

direct visual confirmation of expression to be used as a criterion for cell selection. All the chimeras expressed full-length channels as assessed by Western blot using an anti-GFP antibody (Fig. 2*K*, inset). Cells expressing α_{1G}[cgggg] alone displayed whole-cell currents that were significantly smaller at all test voltages compared to α_{1G} alone channels (Fig. 2*A* and *B*, open symbols; Table 1). When peak amplitudes are compared at −30 mV to ensure a similar driving force, α_{1G}[cgggg] channels exhibited a substantive fourfold decrease in current amplitude (Fig. 2*K*). Co-expressing β_{2a} had no impact on either current amplitude or voltage dependence in this chimeric channel (Fig. 2*A*, *B* and *K*).

In striking contrast to the results obtained with α_{1G}[cgggg], cells expressing α_{1G}[gcggg], a chimera featuring a swap of the entire α_{1C} I–II loop into α_{1G}, demonstrated a dramatic increase in current amplitude and a 30 mV leftward shift in the $I-V$ relationship (Fig. 2*C* and *D*, open symbols; Table 1). When compared at a −30 mV test pulse, α_{1G}[gcggg] channels exhibited an over threefold increase in current density compared to wild-type α_{1G}-alone channels (Fig. 2*F*; $I_{peak} = 62.6 \pm 12.1$ pA pF^{-1}, $n = 12$, for α_{1G}, and $I_{peak} = 197.4 \pm 23.0$ pA pF^{-1}, $n = 8$ for α_{1G}[gcggg] channels, $P < 0.05$, one-way ANOVA). The surprising result with the α_{1G}[gcggg] chimera confirms recent findings (Arias *et al.* 2005; Fan *et al.* 2010), and are seemingly at odds with the notion that the I–II loop of Ca_V1 and Ca_V2 channels harbours a dominant ER retention signal. Co-expressing β_{2a} unexpectedly diminished, rather than increased α_{1G}[gcggg] currents, without affecting the voltage dependence of channel gating (Fig. 2*C*, *D* and *K*; Table 1).

Similar to the results obtained with α_{1G}[cgggg], cells transfected with α_{1G}[ggcgg], α_{1G}[gggcg], or α_{1G}[ggggc] displayed significantly smaller currents compared to wild-type α_{1G}, and were β independent (Fig. 2*E*–*K*; Table 1). Additionally, these other chimeras had only modest, if any, effects on the voltage dependence of channel activation (Table 1). These functional results were not correlated with differences in protein expression (Fig. 2*K*, inset). Overall, these results suggested that no single α_{1C} intracellular domain could confer β-dependent plasma membrane targeting to the α_{1G} backbone. Moreover, the data also raised the radical possibility that the α_{1C} I–II loop could actually facilitate ER export rather than retention in the context of Ca_V channel α_1 subunits. We next sought to test this possibility.

Identification of a putative ER export signal in the α_{1C} I–II loop

It was possible that the variance in current density between wild-type α_{1G} and the single-domain-swapped chimeras was due to changes in channel gating (such as distinctions in channel open probability) rather than differences in channel trafficking. As such, it was important to determine whether the different chimeras displayed divergent propensities to target to the cell surface. Unfortunately, the quantum dot labelling method for surface channels was unsuccessful in the context of $Ca_V3.1$, probably due to geometric constraints that limited accessibility to the surface epitope tag. Fortunately, however, the α_{1G} subunit exhibits robust gating currents, thus rendering it possible to measure Q_{max} as an index of channel trafficking to the membrane. Compared to wild-type α_{1G}, α_{1G}[gcggg] displayed a significantly larger gating current and Q_{max}, while all the other single-domain-swap chimeras (except α_{1G}[ggcgg]) exhibited a diminished Q_{max} (Fig. 3*A*). This result indicates that α_{1G}[gcggg] shows markedly improved membrane targeting, whereas the other chimeras show a relative retention compared to wild-type α_{1G}.

We hypothesized that the α_{1C} I–II loop contains an ER export signal that could potentially explain the enhanced membrane targeting of α_{1G}[gcggg]. Di-acidic motifs (DXD, DXE, EXD and EXE, where X is any amino acid) have been found to act as ER export signals in many membrane proteins (Ma *et al.* 2001; Ma *et al.* 2002; Mikosch & Homann, 2009). We searched for possible acidic residue ER export signals by scanning the α_{1C} I–II loop sequence (Fig. 3*B*; Supplemental Material, Fig. S2). We identified five candidate regions with acidic residue motifs and generated five distinct mutants (termed AXA1–AXA5) in which acidic amino acids (D or E) in the α_{1C} I–II loop were changed to alanine, all within the context of the α_{1G}[gcggg] chimera (Fig. 3*B*). All five chimeras expressed full-length channels (Fig. 3*C*). Whole-cell currents were recorded from HEK 293 cells transfected with each mutant in the absence of β, and $I-V$ curves were generated (Fig. 3*D*). The mutant chimeras AXA1, AXA2, AXA4 and AXA5 displayed current densities that were only modestly reduced compared to α_{1G}[gcggg] (Fig. 3*D*), indicating that the acidic residues present in the associated regions do not account for the ER export capabilities of the α_{1C} I–II loop. By contrast, the mutant chimera AXA3 exhibited a current density that was essentially identical to wild-type α_{1G} (Fig. 3*E*), indicating that the nine acidic residues mutated in this cluster accounted wholly for the increased current density observed with the α_{1G}[gcggg] chimera. Significantly, AXA3 still displayed a $V_{1/2}$ that was substantially left-shifted compared to wild-type α_{1G} (Fig. 3*E*). Therefore, the increase in current density and leftward-shift in activation are separable functions conferred by the α_{1C} I–II loop in the context of α_{1G}[gcggg]. Gating charge analyses (Fig. 3*F*) demonstrated that AXA3 displayed a Q_{max} that was significantly smaller than obtained with α_{1G}[gcggg] ($Q_{max} = 6.01 \pm 1.16$ fC pF^{-1}, $n = 8$ for AXA3, and $Q_{max} = 14.48 \pm 2.83$ fC pF^{-1}, $n = 7$, for α_{1G}[gcggg]-alone channels, $P < 0.05$), and essentially

identical to wild-type α_{1G} ($Q_{max} = 6.95 \pm 1.22$ fC pF^{-1}, $n = 7$). The remaining mutated chimeras (AXA1, AXA2, AXA4 and AXA5), by contrast, exhibited Q_{max} values that were not significantly different from α_{1G}[gcggg] (Fig. 3*F*). Taken together, the results suggest that the acidic residue cluster mutated in AXA3 is a putative ER export region (PEER; Supplemental Material, Fig. S2) in the α_{1C} I–II loop, and that the other α_{1C} intracellular domains may either confer ER retention propensities or increase the rate of channel removal from the cell surface.

Functional interactions among putative α_{1C} ER export and retention modules probed with double and triple domain-substituted chimeras

How do the putative ER retention and export signals functionally interact with each other, and what is the minimum combination of domains required to confer β dependency to channel regulation? To address these questions we generated chimeric channels featuring multiple intracellular domains of α_{1C} swapped into α_{1G}, starting with the 10 possible chimeras

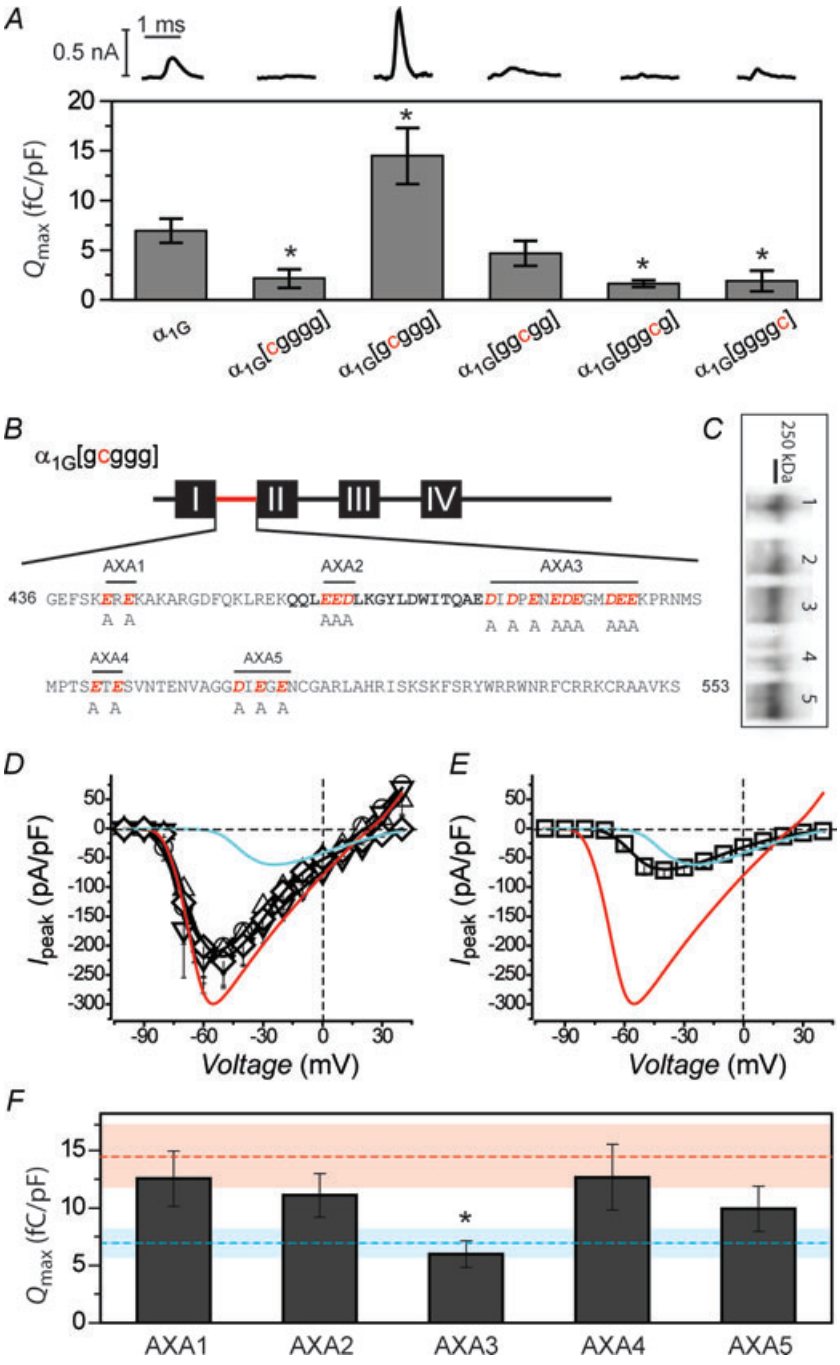

Figure 3. Identification of an acidic sequence that functions as an ER export signal in α_{1C} I–II loop
A, top, exemplar gating currents for wild-type α_{1G} and single domain-substituted chimeric channels. Bottom, comparison of maximal gating charge (Q_{max}) for the different channel types. $^*P < 0.05$ compared to α_{1G}. *B*, sequence of the α_{1C} I–II loop showing candidate acidic-residue ER export signals that were mutated to alanines in the context of the α_{1G}[gcggg] chimera to generate five distinct mutants, AXA1–AXA5. *C*, Western blot: 1, AXA1; 2, AXA2; 3, AXA3; 4, AXA4; 5, AXA5. *D*, population *I–V* curves for chimeric mutant channels AXA1 (○, $n = 9$), AXA2 (△, $n = 6$), AXA4 (▽, $n = 6$) and AXA5 (◇, $n = 6$). Data for wild-type α_{1G} (cyan trace) and α_{1G}[gcggg] (red trace) are reproduced to facilitate visual comparison. *E*, *I–V* curve for AXA3 mutant chimeric channels (□, $n = 8$). *F*, comparison of Q_{max} for the different AXA mutant chimeric channels. Mean data for wild-type α_{1G} (dashed cyan line) and α_{1G}[gcggg] (dashed red line) are represented. $^*P < 0.05$ compared to α_{1G}[gcggg], Wilcoxon's rank sum test.

containing double-domain substitutions (Fig. 4). For these double-domain chimeras, there were two types of questions of primary interest. First, how did the putative ER retention characteristics of the other intracellular domains functionally interact with the export capabilities of the I–II loop? Second, were the putative ER retention properties of individual intracellular domains synergistic when present on the same molecule? Examination of the electrophysiological properties of the four chimeras in which α_{1C} I–II loop was paired with each of the other intracellular domains suggested varying strengths among the distinct ER retention regions (Fig. 4). Cells expressing α_{1G}[ccggg] alone displayed an intermediate current density that lay between wild-type α_{1G} and α_{1G}[gcggg] (Fig. 4*A* and *E*), suggesting α_{1C} N-terminus moderately opposed the ability of the α_{1C} I–II loop to increase channel surface density. Cells expressing α_{1G}[gccgg] alone displayed large currents that were indistinguishable from α_{1G}[gcggg] channels (Fig. 4*B* and *E*), indicating that the α_{1C} II–III loop is unable by itself to diminish the trafficking function of α_{1C} I–II loop. At the other extreme, α_{1G}[gcgcg] and α_{1G}[gcggc] channels exhibited relatively small currents similar in amplitude to wild-type α_{1G} channels (Fig. 4*C*–*E*). Hence, α_{1C} III–IV loop and C-terminus completely neutralized the α_{1C} I–II loop enhanced trafficking effect. All other chimeras that contained two α_{1C} intracellular domains, exclusive of the I–II loop, exhibited exceptionally small currents (Fig. 4*E*; Supplemental Material, Fig. S3). None of the double domain-substituted chimeras showed a β-dependent increase in current density – α_{1G}[gccgg] channels displayed a β-dependent decrease in current density (Fig. 4*B* and *E*) similar to that observed with α_{1G}[gcggg]. These results were not due to differences in protein expression among the distinct chimeric channels (Fig. 4*E*, inset). Overall, these results indicated that the putative ER retention signals on the α_{1C} intracellular loops acted synergistically, and could counteract the propensity of α_{1C} I–II loop to increase channel surface density, but with differing efficacies. Moreover, no two α_{1C} intracellular domains were sufficient to reconstitute β-dependent increased channel trafficking.

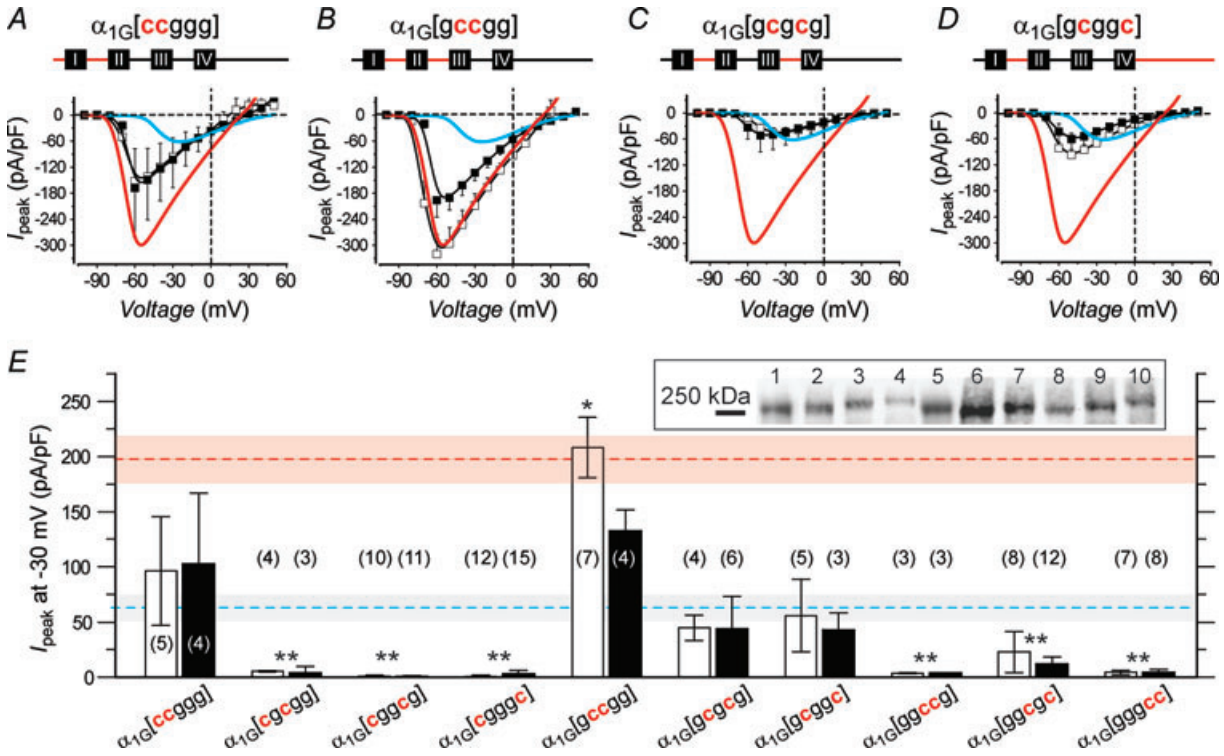

Figure 4. Functional outcomes of chimeras featuring two intracellular domains from α_{1C} substituted into α_{1G}

A–*D*, topological illustrations and population *I*–*V* curves ($\pm\beta$) for those double intracellular domain swapped chimeras that include the α_{1C} I–II loop. Data for wild-type α_{1G} (cyan trace) and α_{1G}[gcggg] (red trace) are reproduced for comparison. *E*, peak current densities acquired at −30 mV for all double intracellular domain swapped chimeras compared to wild-type α_{1G} (dashed cyan line). $^{**}P < 0.005$ for grouped data ($\pm\beta_{2a}$) compared to α_{1G} ($\pm\beta_{2a}$) using one-way ANOVA followed by means comparisons using the Bonferroni test. $^{*}P < 0.001$ compared to α_{1G} ($\pm\beta_{2a}$), one-way ANOVA followed by the Bonferroni test. Inset, Western blot: 1, α_{1G}[ccggg]; 2, α_{1G}[cgcgg]; 3, α_{1G}[cggcg]; 4, α_{1G}[cgggc]; 5, α_{1G}[gccgg]; 6, α_{1G}[gcgcg]; 7, α_{1G}[gcggc]; 8, α_{1G}[ggccg]; 9, α_{1G}[ggcgc]; 10, α_{1G}[gggcc].

These observations were consolidated and extended by considering the functional outcomes of chimeras in which three α_{1C} intracellular domains were swapped into α_{1G} (Fig. 5). All the triple-substituted chimeras which included the α_{1C} I–II loop exhibited currents with amplitudes that were either on par with or less than wild-type α_{1G} (Fig. 5). When the α_{1C} I–II loop was absent, the triple mutant chimeras did not register discernible currents (Fig. 5*G*; Supplemental Material, Fig. S4), consistent with the idea that the discrete putative ER retention signals acted synergistically to retain channels inside the cell. All the triple-substituted chimeras expressed full-length proteins (Fig. 5*G*, inset), and the functional results were not correlated with differences in protein expression. Finally, none of the triple-substituted chimeras displayed β-dependent increase in current density, further

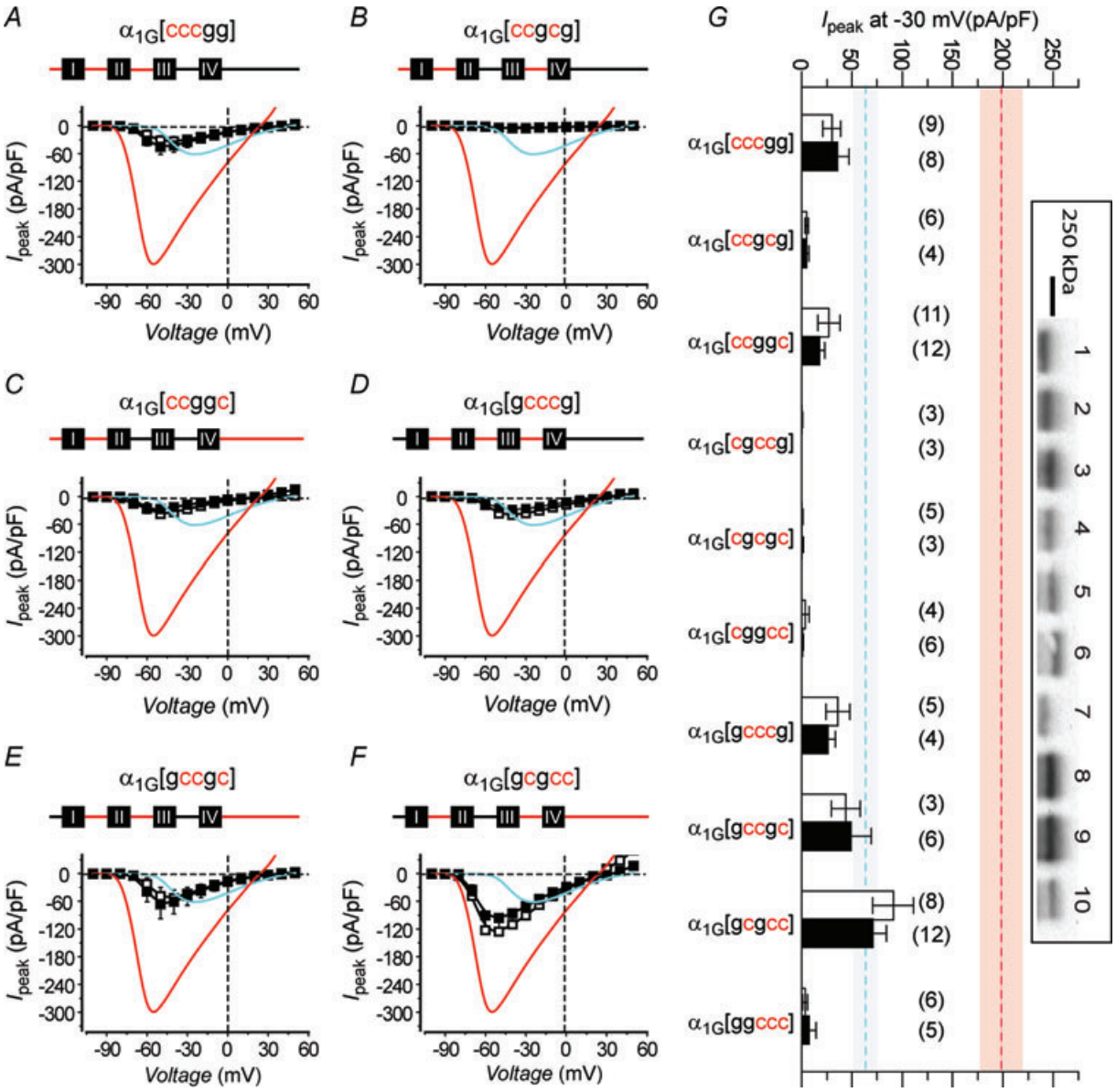

Figure 5. Functional outcomes of chimeras featuring three intracellular domains from α_{1C} substituted into α_{1G}

A–F, topological illustrations and population *I–V* curves ($\pm\beta$) for those triple intracellular domain-swapped chimeras that include the α_{1C} I–II loop. Data for wild-type α_{1G} (cyan trace) and α_{1G}[gcggg] (red trace) are reproduced for comparison. *G*, peak current densities acquired at −30 mV for all triple intracellular domain-swapped chimeras compared to wild-type α_{1G} (dashed cyan line) and α_{1G}[gcggg] channels (dashed red line). $^{**}P < 0.005$ for grouped data ($\pm\beta_{2a}$) compared to α_{1G} ($\pm\beta_{2a}$) using one-way ANOVA followed by means comparisons using the Bonferroni test. Inset, Western blot: 1, α_{1G}[cccgg]; 2, α_{1G}[ccgcg]; 3, α_{1G}[ccggc]; 4, α_{1G}[cgccg]; 5, α_{1G}[cgcgc]; 6, α_{1G}[cggcc]; 7, α_{1G}[gcccg]; 8, α_{1G}[gccgc]; 9, α_{1G}[gcgcc]; 10, α_{1G}[ggccc].

emphasizing the surprisingly complex nature of this phenomenon.

Chimeras displaying successful reconstitution of β-dependent channel regulation

Arguably, the most profound insights into the mechanistic bases of β-dependent channel regulation may be provided by successfully reconstituting this phenomenon in a normally β-independent channel background. As such, it was instructive that three distinct chimeras (α_{1G}[cccgc], α_{1G}[ccgcc] and α_{1G}[gcccc]) characterized by four intracellular domains of α_{1C} substituted into the α_{1G} background recapitulated a β-dependent increase in current density that is normally only seen in Ca_V1/Ca_V2 channels (Fig. 6). Two other quadruple domain-substituted chimeras, α_{1G}[cgccc] and α_{1G}[ccccg], displayed no current in either the absence or presence of β (Fig. 6*A*, *D* and *F*). The fact that α_{1G}[cgccc] produced no currents was not surprising based on the emerging concept that this chimera essentially contains four α_{1C} ER retention modules while lacking the robust ER export services of the α_{1C} I–II loop. Less predictable was the absence of

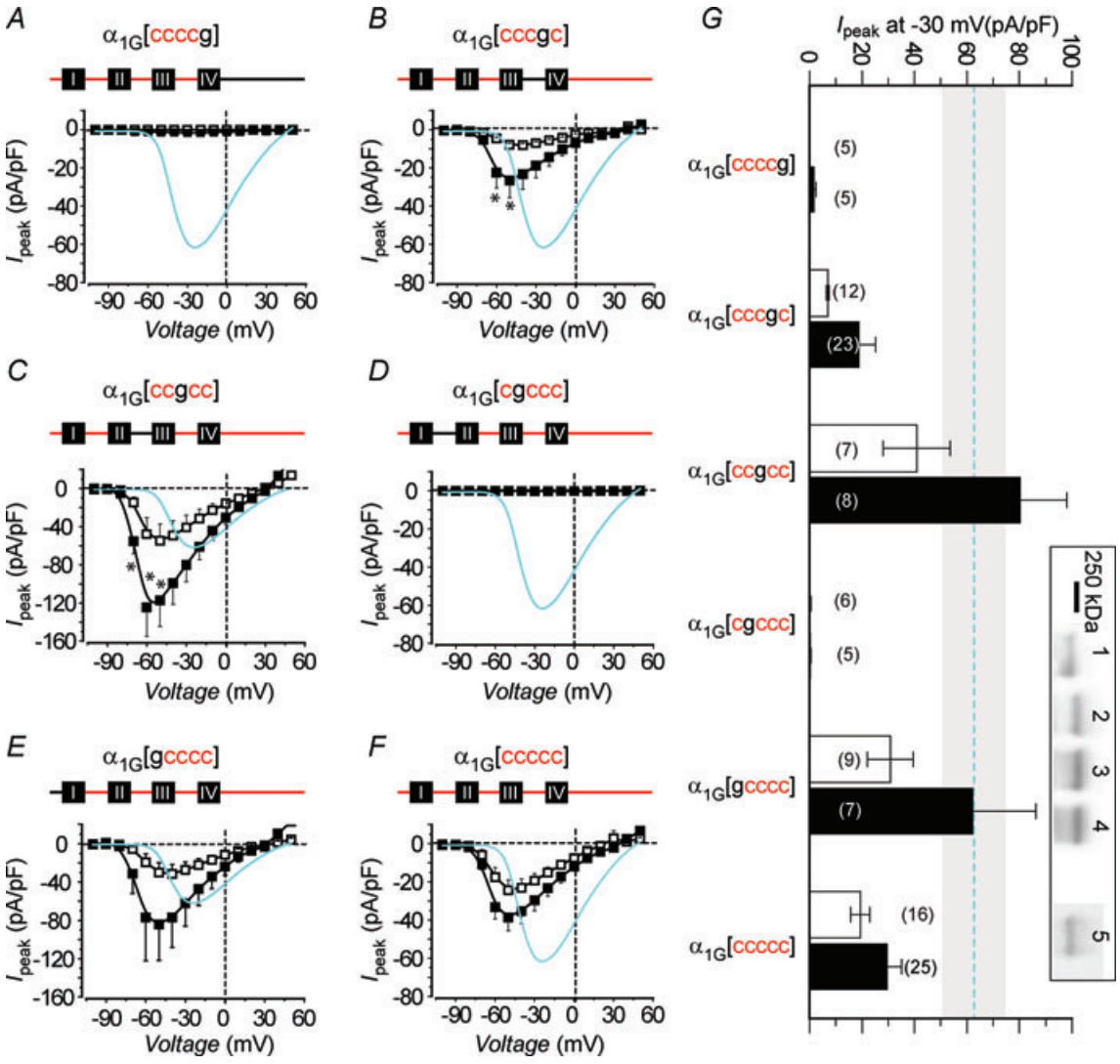

Figure 6. Reconstitution of β regulation of current density in specific chimeric channels containing four α_{1C} intracellular domains swapped into α_{1G}
A–F, topological illustrations and population *I–V* curves ($\pm\beta$) for quadruple and quintuple intracellular domain-swapped chimeras. Data for wild-type α_{1G} (cyan trace) and α_{1G}[gcggg] (red trace) are reproduced for comparison. $^*P < 0.05$ compared to corresponding $-\beta$ data, Wilcoxon's rank sum test. *G*, peak current densities acquired at −30 mV for quadruple and quintuple intracellular domain-swapped chimeras compared to wild-type α_{1G} (dashed cyan line) channels. Inset, Western blot: 1, α_{1G}[ccccg]; 2, α_{1G}[cccgc]; 3, α_{1G}[ccgcc]; 4, α_{1G}[cgccc]; 5, α_{1G}[ccccc].

current observed with the α_{1G}[ccccg] chimera. Together with results from other chimeras, this finding suggests that the α_{1C} C-terminus is absolutely essential for channel trafficking to the membrane and β-dependent channel regulation, but only when it is assembled with at least three other α_{1C} intracellular domains on the same channel molecule. A chimera in which all five intracellular domains of α_{1C} were placed into α_{1G} also displayed currents which trended higher in the presence of β, although this effect did not reach statistical significance (Fig. 6*F* and *G*). All the chimeric channels expressed well (Fig. 6*G*, inset), ruling out differences in protein expression as a potential trivial explanation for the results.

Overall, these results demonstrate that a minimum of four α_{1C} intracellular domains that must include the I–II loop and C-terminus are necessary and sufficient to reconstitute β-dependent regulation of current density in α_{1G}/α_{1C} chimeric channels.

Trafficking role of the I–II loop and C-terminus in the α_{1C} subunit context

Two remaining questions were: (1) does the newly identified PEER in the α_{1C} I–II loop regulate channel surface density in the context of wild-type $Ca_V1.2$ α_{1C} subunit? and (2) how and why is the C-terminus important for $Ca_V1.2$ channel targeting? To address the hypothesized ER export function of the α_{1C} I–II loop in the native channel, we introduced the distinct AXA1–AXA5 mutations (Fig. 3*B*) in the context of α_{1C}[BBS]-YFP (Fig. 7*A*), and monitored channel targeting to the cell surface using the quantum dot labelling method (Fig. 7*B*). Compared to wild-type α_{1C}[BBS]-YFP + β_{2a}, the α_{1C}[AXA3] mutant ($+\beta_{2a}$) exhibited a 60% decrease in QD_{655} fluorescence intensity (Fig. 7*C*), supporting the idea that the PEER is important for channel trafficking within the context of the native $Ca_V1.2$ channel. The fact that β-dependent channel trafficking was not completely abolished in the AXA3 mutant channel may indicate that other ER export signals reside elsewhere on the α_{1C} subunit. Channels bearing mutations of other acidic residues in the I–II loop (AXA2, AXA4 and AXA5) also displayed moderate decreases in trafficking (Fig. 7*C*). However, combining mutations (AXA345) did not decrease the trafficking beyond what was observed with AXA3 alone (data not shown).

The α_{1C} C-terminus is a hub of protein–protein interactions that modulate the $Ca_V1.2$ channel (Supplemental Material, Fig. S5). In particular, the proximal C-termini of Ca_V1 and 2 channels contain pre-IQ and IQ regions (Fig. 7*D*; Supplemental Material, Fig. S5) which serve as binding sites for apo-calmodulin (CaM) and Ca^{2+}–CaM (Romanin *et al.* 2000; Pitt *et al.* 2001; Erickson *et al.* 2003; Kim *et al.* 2004; Van Petegem *et al.* 2005), and are critical for feedback regulation of Ca_V channels (inactivation or facilitation) by Ca^{2+} ions (Lee *et al.* 1999; Peterson *et al.* 1999; Zuhlke *et al.* 1999). Point mutations in the pre-IQ region that ablate apo-CaM binding to the C-terminus also markedly depress β-dependent targeting of the $Ca_V1.2$ channel to the cell surface (Wang *et al.* 2007; Bourdin *et al.* 2010). We sought to gain a deepened appreciation of the role of the α_{1C} C-terminus in $Ca_V1.2$ channel targeting by determining whether the important determinants of β-dependent trafficking were pervasively distributed throughout the C-terminus, or were localized to the pre-IQ/IQ region. Accordingly, we tested the impact of a series of C-terminus truncations on $Ca_V1.2$ channel trafficking to the plasma membrane. Serial truncations at the α_{1C} C-terminus led to graded decreases in $Ca_V1.2$ channel targeting to the cell surface – channels truncated at residues 1906 and 1732 displayed a 60% and 80% reduction in surface density, respectively (Fig. 7*D*). Longer truncations at residues 1632 and 1540, respectively, virtually eliminated β-dependent membrane targeting (Supplemental Material, Fig. S6). Importantly, QD_{655} fluorescence was normalized for YFP expression under all conditions, explicitly ruling out the potential trivial explanation that differences in trafficking propensity among the distinct α_{1C} species could be due to variations in protein expression. Both $\alpha_{1C}\Delta1906$ and $\alpha_{1C}\Delta1732$ functionally retain Ca^{2+}-dependent inactivation (CDI) gating (Erickson *et al.* 2001; Kim *et al.* 2004), as might be expected given that the pre-IQ and IQ regions remain intact (Supplemental Material, Fig. S5). The results indicate that critical determinants of β-dependent trafficking of $Ca_V1.2$ channels are widely distributed throughout the C-terminus, rather than being locally limited to the proximal CaM-binding preIQ/IQ region.

Finally, we examined the impact of combining the α_{1C} I–II loop AXA1–AXA5 mutations and the C-terminus truncations on $Ca_V1.2$ channel trafficking to the cell surface (Fig. 7*E* and *F*). In both $\alpha_{1C}\Delta1906$ and $\alpha_{1C}\Delta1732$, only AXA3 caused a further significant decrease in channel surface density, while the other AXA mutations either caused no change, or even slightly enhanced channel trafficking (Fig. 7*E* and *F*). These results offer further evidence that the PEER in the α_{1C} I–II loop is an important determinant of $Ca_V1.2$ channel surface density.

Discussion

The fundamental importance of auxiliary β subunits to the functional evolution of Ca_V1/Ca_V2 channels is underscored by the severe phenotypes of β-null mice: β_1 – lethal at birth due to asphyxiation (Gregg *et al.* 1996); β_2 – embryonic lethal due to a compromised heartbeat (Ball *et al.* 2002); and β_4 – development of

a *lethargic* epileptic phenotype (Burgess *et al.* 1997). A prominent function of β subunits is to promote the cell surface trafficking of Ca_V1/Ca_V2 channels. In this work we have re-examined the important molecular determinants and mechanism underlying β-subunit-mediated plasma membrane targeting of Ca_V channels. There are three major new findings: (1) the $Ca_V1.2$ α_{1C} subunit I–II loop is a putative ER export rather than retention module; (2)

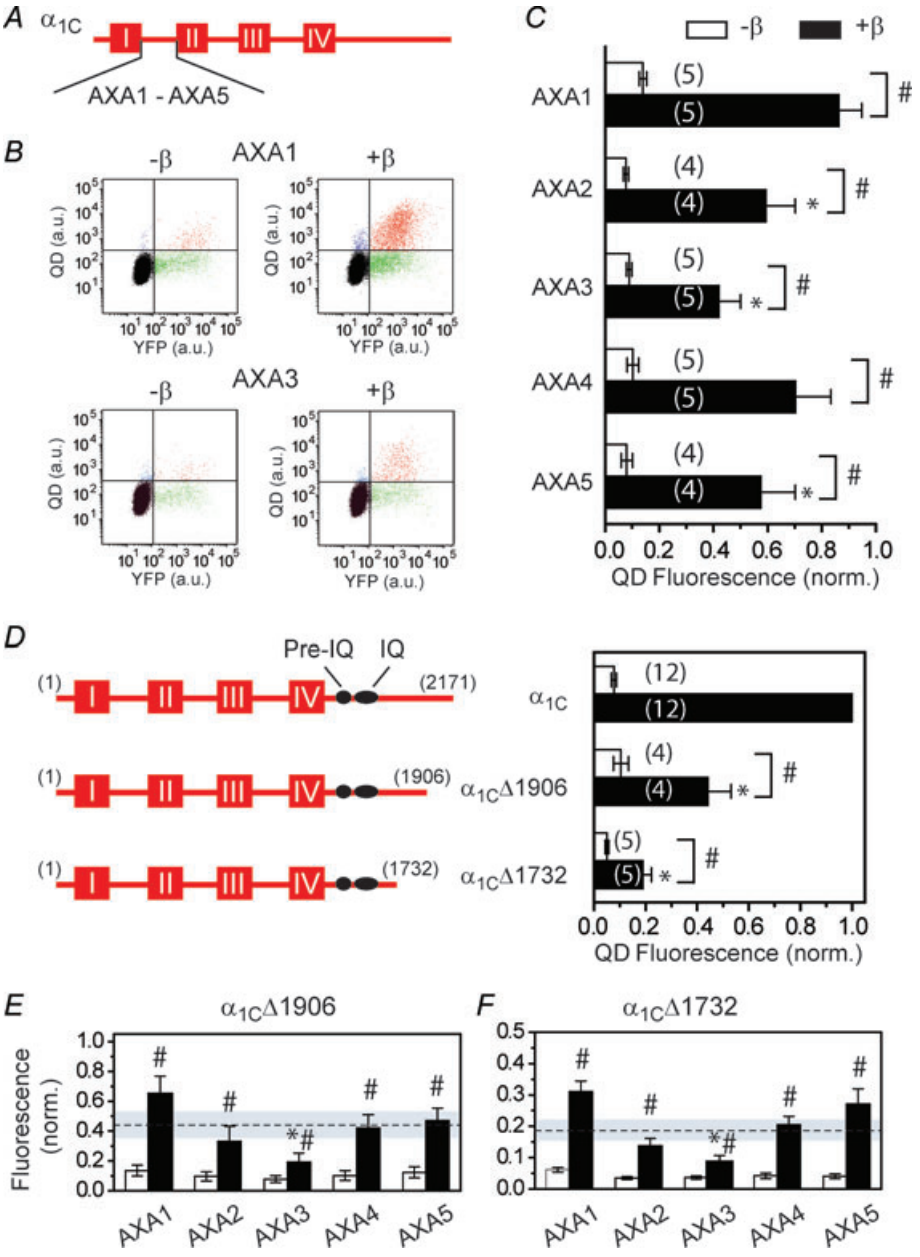

Figure 7. Role of the I–II loop and C-terminus in β-dependent trafficking of $Ca_V1.2$ α_{1C} subunit
A, topological illustration of α_{1C} with AXA1–AXA5 mutations in the I–II loop. *B*, exemplar flow cytometry results examining surface expression of α_{1C}[AXA1] (top) and α_{1C}[AXA3] (bottom) $\pm$ β_{2a} using the quantum dot labelling method. *C*, relative surface expression of (normalized QD_{655} fluorescence intensities) for the distinct α_{1C} AXA mutants. $^*P < 0.05$ compared to α_{1C}[BBS]-YFP + β_{2a}. #$P < 0.05$ compared to the corresponding $-\beta_{2a}$ data. *D*, left, topological illustration of serial C-terminus truncation mutants of α_{1C} showing the relative position of CaM-binding pre-IQ and IQ sites. Right, impact of C-terminus truncations on relative surface expression of α_{1C} subunits $\pm\beta_{2a}$. *E* and *F*, impact of combining C-terminus truncations and AXA1–AXA5 mutations on relative surface expression of α_{1C} subunits, $n = 3$–4. Dashed lines represent means of data for $\alpha_{1C}\Delta1906 + \beta_{2a}$ and $\alpha_{1C}\Delta1732 + \beta_{2a}$, respectively, and the corresponding 95% confidence intervals (shaded regions). $^*P < 0.05$ compared to $\alpha_{1C}\Delta1906 + \beta_{2a}$ and $\alpha_{1C}\Delta1732 + \beta_{2a}$, respectively. #$P < 0.05$ compared to the corresponding $-\beta_{2a}$ data.

the α_1 C-terminus plays a dual role in channel trafficking; and (3) β-dependent increase in channel surface density is an emergent property that requires multiple α_{1C} intracellular domains inclusive of the I–II loop and C-terminus. We discuss these aspects of the work in the context of previous results.

Putative ER export versus retention role of the α_{1C} I–II loop in Ca_V channel trafficking

Auxiliary β subunits bind with nanomolar affinity to the AID in the I–II loop of Ca_V1/Ca_V2 α_1 subunits (Pragnell *et al.* 1994; Canti *et al.* 2001; Opatowsky *et al.* 2003; Butcher *et al.* 2006; Van Petegem *et al.* 2008). High-resolution crystal structures show that β subunits interact with the AID using an α_1-binding pocket formed from non-contiguous residues localized in the GK domain (Chen *et al.* 2004; Opatowsky *et al.* 2004; Van Petegem *et al.* 2004). Point mutations within the AID that disrupt the interaction with β subunits prevent β-induced trafficking of α_1 subunits to the plasma membrane in mammalian cells (Bourdin *et al.* 2010; Obermair *et al.* 2010) and *Xenopus* oocytes (Van Petegem *et al.* 2008). How does β binding to the I–II loop promote trafficking of α_1 subunits to the cell surface? The prevailing notion, based on experiments carried out in $Ca_V2.1$ channels, is that the α_1 subunit I–II loop contains an ER retention signal that becomes masked once β binds, thereby permitting forward trafficking (Bichet *et al.* 2000). The evidence presented in this work suggests that in $Ca_V1.2$ channels the I–II loop does not act as an ER retention module in the context of the Ca_V channel α_1 subunit. Rather, the opposite situation was discovered – i.e. within the context of the channel, the α_{1C} I–II loop may have a net ER export function. A cluster of acidic residues situated just downstream of the AID fully accounted for the capability of the I–II loop to enhance chimeric channel surface density, and reprised a similar function within the context of the native $Ca_V1.2$ channel. It is important to note here that the loss of Ca_V channel trafficking resulting from mutations in the PEER differ fundamentally from previously identified mutations in the I–II loop that also prevent β-induced channel targeting to the cell surface. The previous loss-of-function mutations are within the AID, and prevent channel trafficking by abolishing the $\alpha_1-\beta$ interaction. By contrast, the AXA3 mutations prevent channel trafficking in a β-independent manner, as uniquely demonstrated in the α_{1G}[gcggg] chimeric channel context. Di-acidic ER export motifs have been demonstrated in membrane proteins from plant and animal cells (Ma *et al.* 2001, 2002; Mikosch & Homann, 2009). The basis of their ER export function is believed to be their recognition by components of the coat protein II (COP II) complexes that mediate anterograde ER-to-Golgi vesicular transport (Mikosch & Homann, 2009). We hypothesize that the acidic sequence identified in the α_1 subunit I–II loop may act in such a fashion. This hypothesis will need to be tested in future experiments.

The $Ca_V2.1$ α_1 subunit I–II loop was proposed as an ER retention module based on its ability to retard membrane targeting of either *Shaker* K^+ channels or CD8, when fused to their intracellular C-termini (Bichet *et al.* 2000). However, in similar experiments, neither the $Ca_V1.2$ nor $Ca_V2.2$ α_1 subunit I–II loop displayed ER retention properties, suggesting there may be a genuine difference among distinct Ca_V1/Ca_V2 channel isoforms (Altier *et al.* 2011). Given that the experiments described in this work have focused exclusively on trafficking determinants in $Ca_V1.2$ channels, it is worth considering whether the I–II loop may function similarly in other Ca_V1/Ca_V2 channel types. In this regard, it is reassuring that the I–II loops of both $Ca_V2.2$ (α_{1B}) and $Ca_V2.1$ (α_{1A}) result in a substantial increase in current density when transplanted into to α_{1G} (Arias *et al.* 2005; Fan *et al.* 2010). Moreover, similar to α_{1C}, the α_{1A} and α_{1B} I–II loops contain an acidic residue rich region immediately downstream of the AID (Supplemental Material, Fig. S2). Based on these similarities we speculate that the I–II loop may serve to enhance channel surface density similarly in all Ca_V1/Ca_V2 channels. This prediction will need to be verified experimentally in future experiments.

Role of the α_1 C-terminus in Ca_V channel trafficking

In addition to the I–II loop, there has been accruing evidence that the α_{1C} C-terminus plays a crucial role in Ca_V channel trafficking. Deletion of residues 1623−1666 in the α_{1C} C-terminus abolishes β-dependent trafficking of $Ca_V1.2$ channels to the surface membrane, despite an enduring interaction between the two channel subunits (Gao *et al.* 2000; Bourdin *et al.* 2010). The stretch of deleted amino acids encompasses a demonstrated Ca^{2+}–CaM binding IQ domain (Erickson *et al.* 2003; Kim *et al.* 2004; Van Petegem *et al.* 2005), leading to suggestions that Ca^{2+}–CaM binding to the C-terminus may be necessary for $Ca_V1.2$ channel trafficking to the membrane (Wang *et al.* 2007). However, this idea is challenged by the finding that β-dependent $Ca_V1.2$ channel membrane trafficking remained intact when the α_{1C} subunit featured a more restricted, but still complete, deletion of the IQ domain (residues 1643–1666) (Bourdin *et al.* 2010). On the other hand, point mutations in an upstream pre-IQ site that disrupt apo-CaM binding to the α_{1C} C-terminus also interfere with β-induced membrane targeting of $Ca_V1.2$ channels (Wang *et al.* 2007; Bourdin *et al.* 2010). Hence, apo-CaM, rather than $Ca^{2+}-$CaM, binding to the α_1 C-terminus may be critical for Ca_V channel membrane trafficking. Irrespective of which CaM species is paramount, the question arises as to how CaM molecules can promote β-dependent forward

trafficking of $Ca_V1.2$ channels. It has been previously suggested that the α_{1C} C-terminus may contain an ER retention signal that is masked upon CaM binding, thereby permitting channel movement to the plasma membrane (Wang *et al.* 2007). Further, experiments in which α_{1C} C-terminus fragments were fused to CD4 identified three separate areas in the proximal C-terminus overlapping the EF-hand/pre-IQ/IQ motifs (Supplemental Material, Fig. S5) that exhibited ER retention properties (Altier *et al.* 2011). Aspects of our results support the idea that the α_{1C} C-terminus can function as a net ER retention module. Specifically, when swapped for the analogous domain in α_{1G}, the α_{1C} C-terminus caused a decrease in the surface density of $Ca_V3.1$ channels. Moreover, in the doubly substituted chimera α_{1G}[gcggc], the α_{1C} C-terminus completely neutralized the strong forward trafficking propensity conferred by the α_{1C} I–II loop. Nevertheless, the data also indicate a more complex role of the C-terminus in $Ca_V1.2$ channel trafficking beyond a simple masking of an ER retention sequence by CaM. Truncating α_{1C} at residue 1732 in the C-terminus results in an 80% decrease in channel trafficking even though both $Ca_V\beta$ and CaM still associate with the channel (Gao *et al.* 2000; Erickson *et al.* 2001). This result argues against the simple explanation that CaM merely masks a local ER retention signal, and that this in concert with β binding is sufficient to promote channel trafficking to the membrane. Rather, the data support a more pervasive distribution of determinants on the C-terminus that are important for $Ca_V1.2$ channel trafficking. It is noteworthy that although $\alpha_{1C}\Delta1906$ and $\alpha_{1C}\Delta1732$ target less well than wild-type α_{1C} to the plasma membrane, they typically give rise to larger whole-cell currents in functional assays (Wei *et al.* 1994; Hulme *et al.* 2006). This discrepancy is due to an auto-inhibitory role of the distal C-terminus on channel gating, such that deletion of this region results in a large increase in $Ca_V1.2$ channel P_o (Hulme *et al.* 2006).

Interestingly, the C-termini of the distinct Ca_V1 and 2 channels display little sequence homology beyond the residues corresponding to L1732 in $Ca_V1.2$ (Supplemental Material, Fig. S5). Hence, it is possible that the C-terminus may play divergent roles in β-dependent trafficking among the different channel types. This will be an important and interesting question to address in future studies.

β-dependent trafficking as an emergent property supported by multiple α_1 intracellular domains

A striking result was that the double chimera, α_{1G}[gcggc], which featured both the α_{1C} I–II loop and the C-terminus swapped into α_{1G}, failed to display β-dependent channel targeting to the cell surface. Instead, β-dependent regulation of current density required the presence of at least four intracellular domains of α_{1C} that included the I–II loop and C-terminus. Therefore,

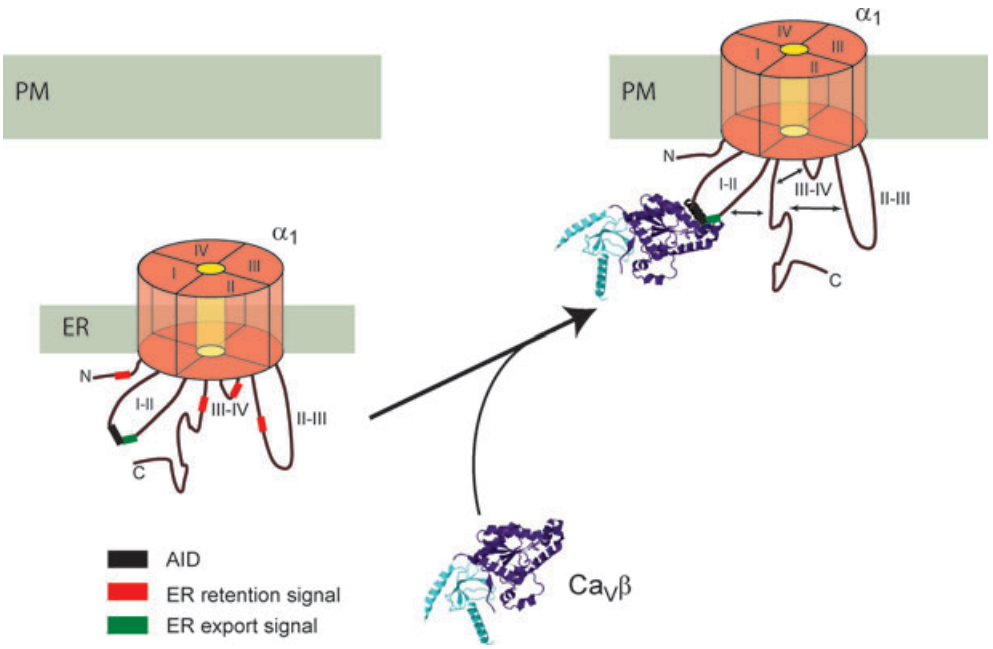

Figure 8. Conceptual model of mechanism underlying β-mediated trafficking of $Ca_V1.2$ channels
In the absence of β, an ER export signal present on the α_1 subunit I–II loop is functionally overcome by discrete ER retention signals present in the other intracellular domains, leading to channels being retained in the ER. Upon β-binding to the α_{1C} I–II loop, a C-terminus-dependent conformational rearrangement of the intracellular domains occurs that diminishes the strength of ER retention signals relative to I–II loop export signals, leading to channel transport to the cell surface.

the α_{1C} I–II loop and C-terminus are necessary but not sufficient to reconstitute β-dependent channel trafficking to the membrane. A limitation of our study is that the magnitude of β-dependent up-regulation of current density reconstituted in the chimeric channels (~three-fold increase) is less than the 10- to 15-fold increase typically observed with wild-type $Ca_V1.2$. A likely contributing factor to this discrepancy is that β subunits increase the single-channel P_o of $Ca_V1.2$ channels (ranging from 2- to 8-fold in different studies) in addition to promoting channel trafficking to the plasma membrane (Kanevsky & Dascal, 2006). The increase in P_o relies on a β-dependent formation of a rigid helix spanning the AID and domain IS6 (Vitko *et al.* 2008; Findeisen & Minor, 2009). Our results do not support a similar β-dependent increase in single channel P_o in the chimeric channels since we do not observe a β-dependent enhancement of current in the majority of chimeras that contain the α_{1C} I–II loop. Hence, the magnitude of β-dependent increase in current density may be quite comparable between the relevant chimeras and $Ca_V1.2$ if the enhanced single-channel P_o effect on the latter is taken into account.

Overall, our results suggest the following hypothesized model for β-dependent regulation of Ca_V channel trafficking (Fig. 8). The α_{1C} I–II loop contains a putative ER export signal while the other intracellular loops and termini have net ER retention characteristics. In the absence of β, the intracellular domains are configured such that the multiple ER retention signals are exposed and functionally dominant, leading to channels being retained in the ER. Upon β-binding to the α_{1C} I–II loop, we propose that a conformational rearrangement of the intracellular domains occurs that diminishes the strength of ER retention signals relative to I–II loop export signals, leading to channel transport to the cell surface (Fig. 8). It is interesting to contemplate the possible nature of the proposed β-induced conformational change in intracellular domains. Our results do not support a model where the β subunit itself physically masks spatially distinct ER retention signals on the channel. If this were the case then it would be expected that β subunits would enhance trafficking in double and triple chimeras that included the I–II loop. However, this was not observed. Rather, the data invite speculation that β-binding to the I–II loop initiates a concerted motion of the intracellular segments that is coordinated by the C-terminus. CaM may participate in this process by promoting a permissive ternary conformation of the C-terminus. This model intimates that the α_{1C} intracellular domains are not independent entities, but rather engage in intra-molecular interactions among themselves. In this regard, it is noteworthy that in $Ca_V2.1$ channels the I–II loop has been demonstrated to interact with the N- and C-termini, and the III–IV loop (Restituito *et al.* 2000; Geib *et al.* 2002). The exact details of the β-induced rearrangement of α_{1C} subunit intracellular segments that we propose will need to be explored in future experiments, including structural studies.

Recently, two groups independently demonstrated that $Ca_V\beta$ binding to either $Ca_V1.2$ (Altier *et al.* 2011) or $Ca_V2.2$ (Waithe *et al.* 2011) protects the respective α_1 subunit from ubiquitination and subsequent proteasomal degradation. In one study, blocking the proteasomal degradation pathway with MG132 was sufficient to rescue surface expression of $Ca_V1.2$ channels even in the absence of β (Altier *et al.* 2011). By contrast, MG132 did not lead to increased surface expression of $Ca_V2.2$ channels in the absence of $Ca_V\beta$ (Waithe *et al.* 2011). Possibly, the β-dependent rearrangement of α_{1C} subunit intracellular segments we envision is necessary to prevent channel ubiquitination and targeting to the proteasome. Further work is clearly needed to reconcile these new results and to develop a more detailed mechanistic model for β regulation of Ca_V1/Ca_V2 channel trafficking.

References

Altier C, Garcia-Caballero A, Simms B, You H, Chen L, Walcher J, Tedford HW, Hermosilla T & Zamponi GW (2011). The Cavβ subunit prevents RFP2-mediated ubiquitination and proteasomal degradation of L-type channels. *Nat Neurosci* **14**, 173–180.

Arias JM, Murbartian J, Vitko I, Lee JH & Perez-Reyes E (2005). Transfer of β subunit regulation from high to low voltage-gated Ca^{2+} channels. *FEBS Lett* **579**, 3907–3912.

Ball SL, Powers PA, Shin HS, Morgans CW, Peachey NS & Gregg RG (2002). Role of the β2 subunit of voltage-dependent calcium channels in the retinal outer plexiform layer. *Invest Ophthalmol Vis Sci* **43**, 1595–1603.

Bers DM (2002). Cardiac excitation-contraction coupling. *Nature* **415**, 198–205.

Bichet D, Cornet V, Geib S, Carlier E, Volsen S, Hoshi T, Mori Y & De Waard M (2000). The I-II loop of the Ca^{2+} channel α1 subunit contains an endoplasmic reticulum retention signal antagonized by the β subunit. *Neuron* **25**, 177–190.

Bourdin B, Marger F, Wall-Lacelle S, Schneider T, Klein H, Sauve R & Parent L (2010). Molecular determinants of the $Ca_V\beta$-induced plasma membrane targeting of the $Ca_V1.2$ channel. *J Biol Chem* **285**, 22853–22863.

Buraei Z & Yang J (2010). The β subunit of voltage-gated Ca^{2+} channels. *Physiol Rev* **90**, 1461–1506.

Burgess DL, Jones JM, Meisler MH & Noebels JL (1997). Mutation of the Ca^{2+} channel β subunit gene *Cchb4* is associated with ataxia and seizures in the lethargic (*lh*) mouse. *Cell* **88**, 385–392.

Butcher AJ, Leroy J, Richards MW, Pratt WS & Dolphin AC (2006). The importance of occupancy rather than affinity of $Ca_V\beta$ subunits for the calcium channel I–II linker in relation to calcium channel function. *J Physiol* **574**, 387–398.

Canti C, Davies A, Berrow NS, Butcher AJ, Page KM & Dolphin AC (2001). Evidence for two concentration-dependent processes for β-subunit effects on α1B calcium channels. *Biophys J* **81**, 1439–1451.

Catterall WA & Few AP (2008). Calcium channel regulation and presynaptic plasticity. *Neuron* **59**, 882–901.

Chen YH, Li MH, Zhang Y, He LL, Yamada Y, Fitzmaurice A, Shen Y, Zhang H, Tong L & Yang J (2004). Structural basis of the α1-β subunit interaction of voltage-gated Ca^{2+} channels. *Nature* **429**, 675–680.

Colecraft HM, Alseikhan B, Takahashi SX, Chaudhuri D, Mittman S, Yegnasubramanian V, Alvania RS, Johns DC, Marban E & Yue DT (2002). Novel functional properties of Ca^{2+} channel β subunits revealed by their expression in adult rat heart cells. *J Physiol* **541**, 435–452.

Cornet V, Bichet D, Sandoz G, Marty I, Brocard J, Bourinet E, Mori Y, Villaz M & De Waard M (2002). Multiple determinants in voltage-dependent P/Q calcium channels control their retention in the endoplasmic reticulum. *Eur J Neurosci* **16**, 883–895.

De Waard M & Campbell KP (1995). Subunit regulation of the neuronal α_{1A} Ca^{2+} channel expressed in *Xenopus* oocytes. *J Physiol* **485**, 619–634.

Deisseroth K, Mermelstein PG, Xia H & Tsien RW (2003). Signaling from synapse to nucleus: the logic behind the mechanisms. *Curr Opin Neurobiol* **13**, 354–365.

Dolphin AC (2003). β subunits of voltage-gated calcium channels. *J Bioenerg Biomembr* **35**, 599–620.

Drummond GB (2009). Reporting ethical matters in *The Journal of Physiology*: standards and advice. *J Physiol* **587**, 713–719.

Erickson MG, Alseikhan BA, Peterson BZ & Yue DT (2001). Preassociation of calmodulin with voltage-gated Ca^{2+} channels revealed by FRET in single living cells. *Neuron* **31**, 973–985.

Erickson MG, Liang H, Mori MX & Yue DT (2003). FRET two-hybrid mapping reveals function and location of L-type Ca^{2+} channel CaM preassociation. *Neuron* **39**, 97–107.

Fakler B & Adelman JP (2008). Control of K_{Ca} channels by calcium nano/microdomains. *Neuron* **59**, 873–881.

Fan M, Buraei Z, Luo HR, Levenson-Palmer R & Yang J (2010). Direct inhibition of P/Q-type voltage-gated Ca^{2+} channels by Gem does not require a direct Gem/$Ca_v\beta$ interaction. *Proc Natl Acad Sci U S A* **107**, 14887–14892.

Findeisen F & Minor DL Jr (2009). Disruption of the IS6-AID linker affects voltage-gated calcium channel inactivation and facilitation. *J Gen Physiol* **133**, 327–343.

Funke L, Dakoji S & Bredt DS (2005). Membrane-associated guanylate kinases regulate adhesion and plasticity at cell junctions. *Annu Rev Biochem* **74**, 219–245.

Gao T, Bunemann M, Gerhardstein BL, Ma H & Hosey MM (2000). Role of the C terminus of the α1C (Ca_V1.2) subunit in membrane targeting of cardiac L-type calcium channels. *J Biol Chem* **275**, 25436–25444.

Gao T, Chien AJ & Hosey MM (1999). Complexes of the α1C and β subunits generate the necessary signal for membrane targeting of class C L-type calcium channels. *J Biol Chem* **274**, 2137–2144.

Geib S, Sandoz G, Cornet V, Mabrouk K, Fund-Saunier O, Bichet D, Villaz M, Hoshi T, Sabatier JM & De Waard M (2002). The interaction between the I-II loop and the III-IV loop of Ca_v2.1 contributes to voltage-dependent inactivation in a β-dependent manner. *J Biol Chem* **277**, 10003–10013.

Gregg RG, Messing A, Strube C, Beurg M, Moss R, Behan M, Sukhareva M, Haynes S, Powell JA, Coronado R & Powers PA (1996). Absence of the β subunit (*cchb1*) of the skeletal muscle dihydropyridine receptor alters expression of the α1 subunit and eliminates excitation-contraction coupling. *Proc Natl Acad Sci U S A* **93**, 13961–13966.

Hulme JT, Yarov-Yarovoy V, Lin TW, Scheuer T & Catterall WA (2006). Autoinhibitory control of the Ca_V1.2 channel by its proteolytically processed distal C-terminal domain. *J Physiol* **576**, 87–102.

Kanevsky N & Dascal N (2006). Regulation of maximal open probability is a separable function of $Ca_v\beta$ subunit in L-type Ca^{2+} channel, dependent on NH_2 terminus of α1C (Ca_v1.2α). *J Gen Physiol* **128**, 15–36.

Kim J, Ghosh S, Nunziato DA & Pitt GS (2004). Identification of the components controlling inactivation of voltage-gated Ca^{2+} channels. *Neuron* **41**, 745–754.

Lee A, Wong ST, Gallagher D, Li B, Storm DR, Scheuer T & Catterall WA (1999). Ca^{2+}/calmodulin binds to and modulates P/Q-type calcium channels. *Nature* **399**, 155–159.

Ma D, Zerangue N, Lin YF, Collins A, Yu M, Jan YN & Jan LY (2001). Role of ER export signals in controlling surface potassium channel numbers. *Science* **291**, 316–319.

Ma D, Zerangue N, Raab-Graham K, Fried SR, Jan YN & Jan LY (2002). Diverse trafficking patterns due to multiple traffic motifs in G protein-activated inwardly rectifying potassium channels from brain and heart. *Neuron* **33**, 715–729.

Mikosch M & Homann U (2009). How do ER export motifs work on ion channel trafficking? *Curr Opin Plant Biol* **12**, 685–689.

Neely A, Wei X, Olcese R, Birnbaumer L & Stefani E (1993). Potentiation by the β subunit of the ratio of the ionic current to the charge movement in the cardiac calcium channel. *Science* **262**, 575–578.

Obermair GJ, Schlick B, Di Biase V, Subramanyam P, Gebhart M, Baumgartner S & Flucher BE (2010). Reciprocal interactions regulate targeting of calcium channel β subunits and membrane expression of α1 subunits in cultured hippocampal neurons. *J Biol Chem* **285**, 5776–5791.

Opatowsky Y, Chen CC, Campbell KP & Hirsch JA (2004). Structural analysis of the voltage-dependent calcium channel β subunit functional core and its complex with the α1 interaction domain. *Neuron* **42**, 387–399.

Opatowsky Y, Chomsky-Hecht O, Kang MG, Campbell KP & Hirsch JA (2003). The voltage-dependent calcium channel β subunit contains two stable interacting domains. *J Biol Chem* **278**, 52323–52332.

Perez-Reyes E, Castellano A, Kim HS, Bertrand P, Baggstrom E, Lacerda AE, Wei XY & Birnbaumer L (1992). Cloning and expression of a cardiac/brain β subunit of the L-type calcium channel. *J Biol Chem* **267**, 1792–1797.

Perez-Reyes E, Cribbs LL, Daud A, Lacerda AE, Barclay J, Williamson MP, Fox M, Rees M & Lee JH (1998). Molecular characterization of a neuronal low-voltage-activated T-type calcium channel. *Nature* **391**, 896–900.

Peterson BZ, DeMaria CD, Adelman JP & Yue DT (1999). Calmodulin is the Ca^{2+} sensor for Ca^{2+}-dependent inactivation of L-type calcium channels. *Neuron* **22**, 549–558.

Pitt GS, Zuhlke RD, Hudmon A, Schulman H, Reuter H & Tsien RW (2001). Molecular basis of calmodulin tethering and Ca^{2+}-dependent inactivation of L-type Ca^{2+} channels. *J Biol Chem* **276**, 30794–30802.

Pragnell M, De Waard M, Mori Y, Tanabe T, Snutch TP & Campbell KP (1994). Calcium channel β-subunit binds to a conserved motif in the I-II cytoplasmic linker of the α1-subunit. *Nature* **368**, 67–70.

Restituito S, Cens T, Barrere C, Geib S, Galas S, De Waard M & Charnet P (2000). The β2a subunit is a molecular groom for the Ca^{2+} channel inactivation gate. *J Neurosci* **20**, 9046–9052.

Romanin C, Gamsjaeger R, Kahr H, Schaufler D, Carlson O, Abernethy DR & Soldatov NM (2000). Ca^{2+} sensors of L-type Ca^{2+} channel. *FEBS Lett* **487**, 301–306.

Sekine-Aizawa Y & Huganir RL (2004). Imaging of receptor trafficking by using α-bungarotoxin-binding-site-tagged receptors. *Proc Natl Acad Sci U S A* **101**, 17114–17119.

Takahashi SX, Miriyala J & Colecraft HM (2004). Membrane-associated guanylate kinase-like properties of β-subunits required for modulation of voltage-dependent Ca^{2+} channels. *Proc Natl Acad Sci U S A* **101**, 7193–7198.

Van Petegem F, Chatelain FC & Minor DL Jr (2005). Insights into voltage-gated calcium channel regulation from the structure of the $Ca_V1.2$ IQ domain-Ca^{2+}/calmodulin complex. *Nat Struct Mol Biol* **12**, 1108–1115.

Van Petegem F, Clark KA, Chatelain FC & Minor DL Jr (2004). Structure of a complex between a voltage-gated calcium channel β-subunit and an α-subunit domain. *Nature* **429**, 671–675.

Van Petegem F, Duderstadt KE, Clark KA, Wang M & Minor DL Jr (2008). Alanine-scanning mutagenesis defines a conserved energetic hotspot in the $Ca_V\alpha1$ AID-$Ca_V\beta$ interaction site that is critical for channel modulation. *Structure* **16**, 280–294.

Vitko I, Shcheglovitov A, Baumgart JP, Arias O II, Murbartian J, Arias JM & Perez-Reyes E (2008). Orientation of the calcium channel b relative to the $\alpha_1$2.2 subunit is critical for its regulation of channel activity. *PLoS ONE* **3**, e3560.

Waithe D, Ferron L, Page KM, Chaggar K & Dolphin AC (2011). β-subunits promote the expression of $Ca_V2.2$ channels by reducing their proteasomal degradation. *J Biol Chem* **286**, 9598–9611.

Wang HG, George MS, Kim J, Wang C & Pitt GS (2007). Ca^{2+}/calmodulin regulates trafficking of $Ca_V1.2$ Ca^{2+} channels in cultured hippocampal neurons. *J Neurosci* **27**, 9086–9093.

Wei X, Neely A, Lacerda AE, Olcese R, Stefani E, Perez-Reyes E & Birnbaumer L (1994). Modification of Ca^{2+} channel activity by deletions at the carboxyl terminus of the cardiac α1 subunit. *J Biol Chem* **269**, 1635–1640.

Yang T, Xu X, Kernan T, Wu V & Colecraft HM (2010). Rem, a member of the RGK GTPases, inhibits recombinant $Ca_V1.2$ channels using multiple mechanisms that require distinct conformations of the GTPase. *J Physiol* **588**, 1665–1681.

Zuhlke RD, Pitt GS, Deisseroth K, Tsien RW & Reuter H (1999). Calmodulin supports both inactivation and facilitation of L-type calcium channels. *Nature* **399**, 159–162.

Author contributions

K.F. designed and conducted experiments in all areas of the work, analysed results, interpreted data, and helped write the paper. H.M.C. conceived of and designed experiments, analysed results, interpreted data, and wrote the paper. Both authors approved the final version of the manuscript.

Acknowledgements

The authors thank Ming Chen and Timothy Kernan for technical assistance; Dr Ed Perez-Reyes (University of Virginia) for the rat α_{1G} clone; and Drs Prakash Subramanyam and Xianghua Xu for comments on the manuscript. This work was supported by grants from the National Institutes of Health (RO1 HL069911 and RO1 HL084332) to H.M.C. H.M.C. is an Established Investigator of the American Heart Association.